CHALMERS
UNIVERSITY OF TECHNOLOGY

Simulations of Dielectric Frequency Response of Bushings for a Non-Destructive On-site Defect Identification

Master's thesis in Sustainable Electric Power Engineering and Electromobility

NIGALYADEVI KULANDAIVEL

DEPARTMENT OF ELECTRICAL ENGINEERING

CHALMERS UNIVERSITY OF TECHNOLOGY
Gothenburg, Sweden 2025
www.chalmers.se

Master's thesis in Electric Power Engineering 2025

Simulations of Dielectric Frequency Response of Bushings for a Non-Destructive On-site Defect Identification

NIGALYADEVI KULANDAIVEL

CHALMERS
UNIVERSITY OF TECHNOLOGY

Department of Electrical Engineering
Division of Electric Power Engineering
Chalmers University of Technology
Gothenburg, Sweden 2025

Simulations of Dielectric Frequency Response of Bushings for a Non-Destructive On-site Defect Identification

Supervisor: Christos Athanasopoulos, R&D Principal Engineer,
Hitachi Energy Sweden AB, Ludvika, Sweden
Examiner: Prof. Yuriy Serdyuk, Professor, Electric Power Engineering
Chalmers University of Technology, Gothenburg, Sweden

Master's Thesis 2025
Department of Electrical Engineering
Division of Electric Power Engineering
Chalmers University of Technology
SE-412 96 Gothenburg
Telephone +46 31 772 1000

Cover: High Voltage Transformer Bushings.

Typeset in LaTeX

Simulations of Dielectric Frequency Response of Bushings for a Non-Destructive On-site Defect Identification
NIGALYADEVI KULANDAIVEL
Department of Electrical Engineering
Chalmers University of Technology

Abstract

Bushings are integrated components of high voltage transformers providing connections of windings to external circuits outside the transformer shell while providing mechanical and insulation support. During normal operation, bushings are consistently influenced by operating voltage, load current, and voltage stress due to transient over-voltages during natural or switching phenomena in the power system network. These stresses gradually degrade the bushing insulation and eventually cause failure, The insulation state should be monitored and maintained periodically. Dielectric Frequency Response (DFR) measurements yielding capacitance and loss factor values in frequency domain is one of the most popular diagnostics methods, which provides fruitful information about insulation conditions and possible defects that may be present within the bushing insulation.

The aim of the thesis project is to develop a transformer bushing model using COMSOL Multiphysics to perform simulations of DFR for a real scale transform bushing geometry. The model was implemented based on electrostatics physics and current continuity through the insulation structure. The loss factor and the capacitance values were computed in the frequency window typical for practical measurements. The results of the simulations conducted using the developed model are validated by comparing them with measured DFR data. Furthermore, possible defects, which may appear in practice (conductive layers on the insulation, gas bubbles in the insulation bulk) were introduced in the model and frequency dependent loss factor and capacitance values were computed for each type of defects. The results are compared with the reference (defect free) case to identify and interpret the dielectric response behavior. The sensitivity study conducted by varying the properties of the defects indicate that the developed model provides a tool for capturing presence of defects in the insulation by analyzing changes in the DF response.

Keywords: Dissipation Factor, Dielectric Loss, Dielectric Frequency Response, Capacitance

Acknowledgements

I would like to express my heartfelt gratitude to Ana-Paula Ribeiro, R&D Manager, Bushings, Francisco Penayo, R&D Engineer, Bushings, and Christos Athanasopoulos,R&D Principal Engineer, Bushings at Hitachi Energy Sweden AB for providing me this thesis opportunity and for their continuous support during the entire master thesis period at Ludvika.

I extend my genuine gratefulness to Christos for being my thesis supervisor and greatly motivating me to keep moving forward with the project. His incredible years of experience in Bushing technology greatly helped to take the thesis work in the right direction and carry out the work effectively. His kindness and positive approach constantly being my great inspiration in this thesis journey.

I also extend my sincere thanks to the entire R&D Bushings team for providing me the supportive and inclusive work space to carry out the thesis successfully.

Furthermore, I would like to express my deepest gratitude to my examiner and supervisor Prof. Yuriy Serdyuk for being my consistent support and provided me with right guidance throughout this journey. I am really admired by his exceptional years of expertise in High Voltage Technology which incredibly helped me to handle the challenges and confidently progress with the thesis project.

Lastly, I always remain deeply grateful to my beloved family and my friend Sibi Pranav Rajarajan for supporting me through thick and think and having confidence on me, this journey wouldn't be possible without their love and support.

Nigalyadevi Kulandaivel, Gothenburg, June 2025

List of Acronyms

Below is the list of acronyms that have been used throughout this thesis listed in alphabetical order:

DFR	Dielectric Frequency Response
FDS	Frequency Domain Spectroscopy
HV	High Voltage
IEEE	Institute of Electrical and Electronics Engineers
IEC	International Electrotechnical Commission
CIGRE	Council on Large Electric Systems
PD	Partial Discharge
PF	Power Factor
LFPF	Line Frequency Power Factor
DF	Dissipation Factor
RBP	Resin-Bonded Paper Bushing
OIP	Oil Impregnated Paper Bushing
RIP	Resin-Impregnated Paper Bushing
RIS	Resin-Impregnated Synthetics Bushing
FEM	Finite Element Method
ITC	Individual Temperature Correction
GSU	Generator Step-Up

Contents

List of Figures

List of Tables

1
Introduction

1.1 Transformers in Power System

In this technology-driven world, electricity is the backbone for every individual on Earth to run day-to-day life in a hassle-free manner, with which the following fact cannot be denied: "Without electricity, the wheels of the world will stop". To ensure a continuous supply of electricity to consumers, it is important to ensure the stable and reliable operation of the entire power system network from its generation to transmission to its distribution. The electrical power system network comprises of several High Voltage (HV) components such as Transformers, Lightning Arresters, Isolators, Instrument Transformers, Transmission lines, Circuit Breakers, etc. The stability of the power system depends on the reliable operation of the HV components while withstanding the electrical, thermal, and mechanical stresses. The performance of the HV component depends on the withstanding Capability of its insulation system during normal operation and faulty condition.

Figure 1.1: Power Transformer [1]

Among all other HV equipment, Transformers form an integral part of the Generation, transmission, and distribution of the electrical power network. A transformer is a static device that transfers electrical energy from one voltage level to another using the principle of electromagnetic induction [2]. The transformer primarily con-

sists of a core, windings, Oil, winding insulation system, a conservator tank, and a cooling system. There are different types of transformers depending on the type of application. For example, transformers used in the transmission network as *Power Transformers*, used to generate test voltages and test currents as *Test transformers*, and to measure currents and voltages as *Instrument Transformers*. In recent years,transformers as *Converter Transformers* play a vital role in enabling HVDC transmission technology and renewable energy integration [4].

At highest voltage levels, they are expensive and become a strategically important component in the electrical power system network [4]. It is installed at various sections of the power system, ranging from few tens of KVA to several hundreds of MVA with capital of hundreds to several million dollars. Hence, reliable operation, longer life, reduced replacement and maintenance cost of transformers are highly correlated with the stability and reliability of the electrical power system [11]. The main parts of the windings, core, and insulation system for the windings. The important accessories of the power transformers are Cooling Unit, Conservator Tank, Silica Gel Breather, Bushings, Tap Changers, Buchholz Relay, Pressure Relief Valve, Oil gauge, and temperature indicators [12].

The Average Life span of power transformers which is shown in the Figure 1.1 is defined between 25 and 40 years. They undergo high electrical and thermal stresses during the normal operation. Although transformers are highly energy efficient, the amount of heat dissipation limits their maximum loading [3] [1]. Various internal and external causes lead to transformer failure, which disturbs the overall reliability of the power system. The major cause of the transformer failure is caused due to the winding-related failures, contributing to 36.7 % as shown in the Figure. Besides,the other major contributors to the transformer failure are caused by the bushing accounting to 24.9 % and Tap Changers, to 18.8 % [13] [14]. The statistics for the location of all major failures is shown in the Figure 1.2 [13]. Bushing failure often lead to severe effects of explosion and fire [13].

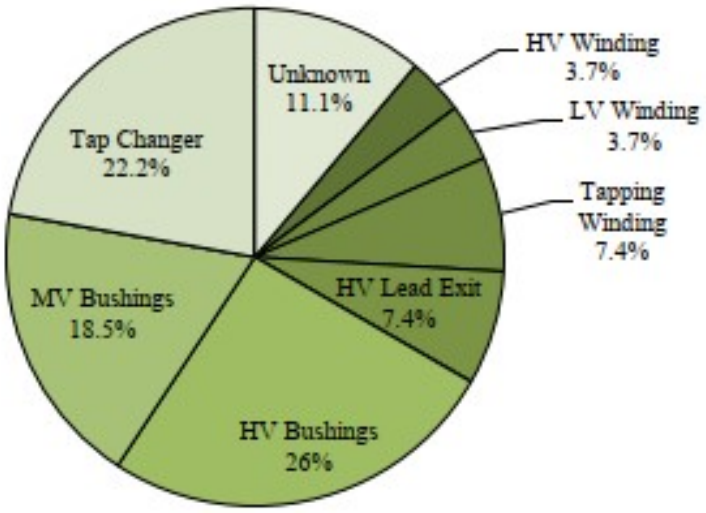

Figure 1.2: Failure Locations of major transformer failure [13]

1.2 Bushing Insulation monitoring

In transformers, bushings form an integral component that conducts current outside the transformer shell while providing mechanical and insulation support. As mentioned in the previous section 1.1, bushing failure is one of the significant cause in the case of major transformer failure. It contributes to approximately 15-30% of transformer outages globally as per the statistics published in IEEE, IEC and CIGRE. Around 40% events of the bushing failure are of domineering that result in calamitous events such as fire, explosion or rupture of transformer tank. Besides, the 30% of failures in Generator Step-Up (GSU) Transformers are caused due to the improper function of bushings [15]. Therefore, it is of high priority to monitor the bushing health to ensure its normal function so that the catastrophic event of failures can be prevented during its lifetime. This brings up high importance to the transformer operators to assess the bushing condition, specifically the insulation system of bushings. Bushings are generally manufactured with a current carrying central conductor, that is wounded successively with conductive layers and insulating paper [15].

(a) Discharge in Bushing Core [15]

(b) Bushing Explosion [17]

Figure 1.3: Failure Conditions in Bushing

During the normal operation, bushings are consistently influenced by operating voltage, load current, and voltage stress due to transient over-voltages during natural or switching phenomena in the power system network. They are designed in such a way it could withstand electrical, thermal, mechanical and ambient stresses during its normal operating condition [10]. These stresses gradually degrade the bushing insulation and eventually cause failure if not monitored and maintained periodically. The bushing failure is accompanied by an explosion that could cause severe damage to adjacent equipment, power outages, and nearby working personnel. An example of bushing explosion in the event of failure is shown in the Figure 1.3b [17] and the Figure 1.3a shows the discharge in the bushing core due to the detachment of conductive strip that connects the first foil layer. [15] Therefore, the bushing insulation should withstand the operational stresses to ensure the reliable operation of

the transformer and other power system equipment in the network.

To ensure the safe operation of bushings under permissible stress limits, monitoring and maintaining the bushing periodically is necessary. All the bushings need to be monitored periodically for 3-5 years. In any case, bushings that exhibit signs of degradation should be tested in the intervals of 6 months to 1 year and removed from the service if it has potentially led to bushing failure. By using non-destructive methods of testing, the earlier identification of any potential causes that lead to deterioration of bushing insulation can be identified. The advantage of these non-destructive methods at on-site diagnose the condition of the bushing without being removed from its normal operation. The common cause of Bushing insulation failure is caused by the gradual build-up of moisture ingression in bushing insulation system. One such advanced diagnostic tool is *Dielectric Frequency Response (DFR)* which helps to assess the condition of the combined insulation system inside the bushing. The result obtained from this tool is the representation of dielectric response in the frequency domain and it is otherwise known as Frequency Domain Spectroscopy(FDS).

1.3 Objectives and scope of the Thesis

The thesis project on DFR simulations will be carried out at Hitachi Energy Sweden AB in Ludvika under the supervision of Christos Athanasopoulos. The thesis project aims to develop and enhance an existing model using COMSOL Multiphysics to perform electrical simulations of transformer bushings in the frequency domain.

The main objective is to simulate Dielectric Frequency Response (DFR) measurements, which are widely used to assess the condition of insulation system in bushings. The project involves validating the bushing model by comparing the simulation results with measured data. Comparing the obtained dielectric spectrum with the DFR measurements helps in early identification of defects in the bushing insulation system. The interpretation provides useful information to find early signs of any incipient fault in the bushing insulation. The deliverables of the project is to arrive at working COMSOL model, a technical report and a presentation of the work to the R&D Bushings team at Hitachi Energy and at Chalmers University of Technology.

The scope of the thesis is to develop and improve an existing bushing model in COMSOL Multiphysics to perform the DFR simulations for the chosen bushing configuration. The frequency spectra is obtained by importing data into COMSOL from existing DFR measurements conducted according to the IEEE Std C57.161™-2018. Further, the results are then compared with the DFR measurements to analyze for any distortions in the resultant response which indicates the early sign of deterioration in the bushing insulation.

2

Theory

2.1 High Voltage Bushings

According to the standard IEC 60137, the Bushing is defined as "device that enables one or several conductors to pass through a partition such as a wall or a tank, and insulates the conductors from it; the means of attachment (flange or fixing device) to the partition forms part of the bushing" [8]. ANSI/IEEE Std. C57.19.00 defined bushing as “an insulating structure, including a through conductor or providing a central passage for such a conductor, with provision for mounting a barrier, conducting or otherwise, for the purpose of insulating the conductor from the barrier and conducting current from one side of the barrier to the other” [7]. In other words, the bushings consist of one or more high-voltage conductors to pass through an earthed barrier such as the tank of a transformer or wall [5]. The purpose of the bushing is to provide the mechanical and electrical support for the device where it is installed, such as walls, substations, transformers, and generators [4]. During normal operation or when experiencing service over voltages, it must provide electrical insulation support. It also offers better mechanical support for the HV conductors and external connections [10] [5]. The bushing must be capable of withstand stresses during testing and operation, which implies that it satisfies the same purpose as cable termination in cables [4]. The insulation of the bushing must be capable to endure the applied voltage and the conductor must be able to carry its rated current without causing overheat of neighboring insulation structure [6].

2.2 Types of Bushings

The configurations of the bushings vary depending on their rated voltage, its application, and the insulating materials. There are different methods to classify, whereas the following classifications are based on their application in real time [6]. The classification are as follows

1. Based on the Insulation media on the ends
2. Based on the construction

2.2.1 Based on the Insulation media on the ends

These category mainly depends on the end application of bushings.

2.2.1.1 Air to Oil bushings

This type of bushing has two different insulation media on its ends. One end of the bushing is air, and the other end of the bushing is oil. The length of the oil side is less compared to that of the air side as the dielectric strength of oil is greater than that of the air at atmospheric pressure. This type is generally used for applications where the bushing is required to be installed between an air and an oil-filled device, e.g. Transformers [6]. The transformer bushing, which is of Air to Oil type, is shown in the Figure 2.1 [18].

Figure 2.1: Air to Oil - Transformer Bushing [18]

2.2.1.2 Air to Air bushings

This bushing type has the same insulation media as air on both ends. One end of the bushing is exposed to atmospheric air, whereas the other side is exposed to indoor. The creepage length of the air side that is exposed to outdoors is higher than the end exposed to indoors. This is because the outdoor end should exhibit higher resistance towards the highly polluted environmental conditions. Besides, the strike distance is also higher to withstand the transient overvoltages during bad weather circumstances. This type is generally used for applications where the bushing is required to be installed in buildings [6]. The wall bushing which is of Air to Air type, is shown in the Figure 2.2 [19].

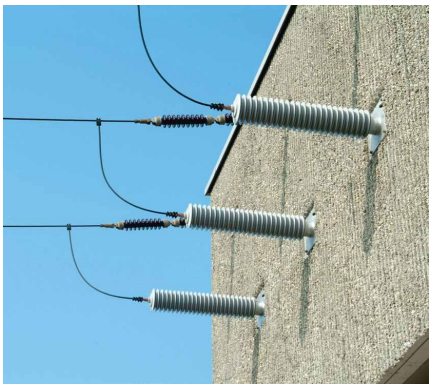

Figure 2.2: Air to Air - Wall Bushing [19]

2.2.1.3 Special Applications

Some bushings are only used for some specific applications such as Air to SF_6 bushings for SF_6 circuit breakers, Oil to oil bushings are used in between oil bus ducts and oil-filled device and Oil to SF_6 bushings are installed between SF bus ducts and oil-filled device [6]. The gas bushing which is of Air to SF_6 type, is shown in the Figure 2.3 [20].

Figure 2.3: Air to SF_6 bushing [20]

2.2.2 Based on the construction

Based on construction, the bushings are classified into two types as follows

1. Solid or Non Condenser Bushing
2. Condenser or Capacitance Graded Bushing

2.2.2.1 Solid bushings

The construction of a solid bushing which is shown in the Figure 2.4 is simpler than that of a condenser-type bushing. It consists of a single central conductor surrounded by a cylindrical housing of insulation materials like porcelain, epoxy, glass, paper, cast resin, etc. This type of bushing is used in smaller kV distribution transformers, in switching circuits for higher MVA generator step-up transformers, and in power generators with coolant as hydrogen.

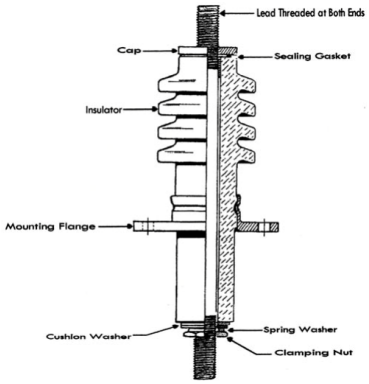

Figure 2.4: Solid Bushing [6]

For lower kV solid bushings, the gap between the conductor and the insulating materials is filled with air, whereas for higher kV, it may contain electrically graded mineral oil or some type of special compound. In the case of oil-filled, it may be encased within the bushing or from the device to which the bushing is installed. In the case of the special compound, it is commonly contained within the bushing. The usage of the oil and other compounds is due to their better cooling characteristic, provide higher dielectric strength than air and have higher breakdown strength. This increases its capability to withstand over voltage during its operation.
Solid bushings cannot be used for application that requires withstanding 60Hz voltages greater than 90 kV. It is well suited for lower kV applications and is cost-effective as well. In recent days, the usage of solid type is limited to meet the lower partial discharge values during the testing of the transformer. Additionally, the non-uniform distribution of the electric field in both radial and axial direction, makes it inappropriate for high-voltage applications [6] [5] [10].

2.2.2.2 Condenser or Capacitance Graded bushings

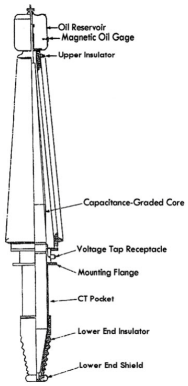

(a) Construction of Capacitance Graded Bushing - Oil filled [6]

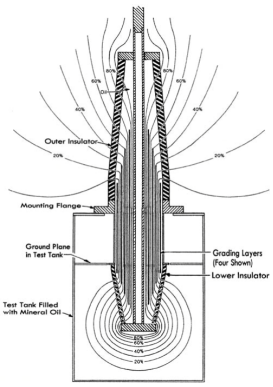

(b) Equipotential lines in Capacitance graded bushing [6]

Figure 2.5: Condenser or Capacitance graded Bushing

The standard ANSI/IEEE Std. C57.19.00 defines the capacitance graded bushings as "in which metallic or non-metallic conducting layers are arranged within the insulating material for the purpose of controlling the distribution of the electric field of the bushing, both axially and radially" [7]. The construction of this type is different from solid type as shown in the Figure 2.5a and it consists of central conductor wounded by insulating paper with conductive layer inserted at predefined intervals in radial direction. The purpose of placing the conductive layers within paper insulation is to form the concentric capacitance in series to obtain uniform electric potential distribution inside the bushings as shown in the Figure 2.5b. The capacitance is distributed between the conductive layers in such a way that uniform

electric field distribution is achieved.These alternative layers of conductive layers and paper are contained in the space between the central conductor and the outer insulator. The construction of the bushing condenser core that showcases the formation of series capacitance is shown in the Figure 2.6 [22]. The term test tap and the capacitance C1, C2 will be discussed in the upcoming sections.

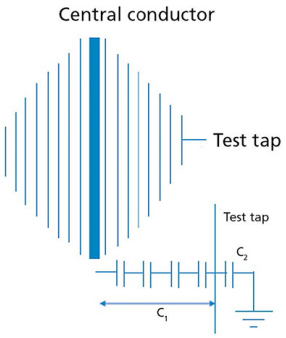

Figure 2.6: Simplified Representation of Condenser Core [22]

In earlier days, the series capacitance was formed by inserting concentric cylinders made of porcelain with metalized surfaces or tubular shaped press boards with conductive layers enclosed in it. In recent years, most of the bushing manufacturers use conductive of aluminium or copper along with oil-impregnated kraft-paper [6] [5]. The other alternatives are conductive paint, printed semi conductive ink, or semi conductive paper [6]. In Hitachi Energy Sweden AB, conductive layers in all the types of bushings are made of aluminium foils hence in the upcoming sections, the term "foils" will be used instead and is originally referred to "conductive layer". The axial length of the adjacent foils is different so that the potential is equally distributed along the surface of the bushing [10]. There are four different classifications of condenser bushing.

1. Resin-Bonded Paper Bushing RBP
2. Oil Impregnated Paper Bushing OIP
3. Resin-Impregnated Paper Bushing RIP
4. Resin-Impregnated Synthetics Bushing RIS

(a) Resin-Bonded Paper Bushing RBP

In this type of bushing, the core of the bushing is wounded with paper which is coated with resin. The each layer of paper is secured to the previous layer by the coated resin. Subsequently, the bushing core undergoes curing process to achieve the bonding between foils. During manufacturing, improper curing causes the formation of voids in the paper insulation and thus resulting in PD. This can be one of the cause of bushing failure in the long run [7] [10].

(b) Oil Impregnated Paper Bushing OIP

In this type of bushing, the core of the bushing is wounded with paper and eventually it is impregnated with oil. The space between the OIP insulated core and the outer insulation is also filled with oil [7]. The Partial Discharge (PD) inception voltage of OIP bushing will be higher than RBP bushing when there are no gas

cavities present inside the bushing insulation oil. This can be achieved through precise manufacturing process. Some cases like the misplacement of conductive layers can cause the increased electric field stress at the ends of the layers. Because of the higher stress, discharges can occur and results in formation of gas cavities in the oil, eventually it causes breakdown [10].

(C) Resin Impregnated Paper Bushing RIP
In this type of bushing, the core of the bushing is wounded with untreated paper and it is vacuum impregnated with curable resin [7]. The advantages of RIP bushing are free of voids, gas tight, and dry in nature as the paper wounded core is vacuum impregnated. Eventually, it has lower dielectric losses and PD free [10].

(d) Resin Impregnated Synthetic Bushing RIS
In this type of bushing, the core of the bushing is wounded with synthetic poymer and it is impregnated with curable resin [7].

The bushing presented in this thesis work is Transformer Bushing which comes under Air - Oil type based on its application and RIP Insulated based on its construction.

2.3 Parts of Bushing

The main parts of the presented transformer bushing are condenser core, Outer Insulation, flange, Oil reservoir, and corona shield. The condenser core comprises of conductor and RIP Insulation part [12]. It is significant that the bushing design must ensure that it is capable of withstanding all kinds of stresses during the operation and testing. Capacitance graded bushings are generally installed for high voltage applications. The maximum stress that can be handled by each material is found to be during its test and maintenance events. This helps in bringing up the efficient bushing design at all levels so that the life expectancy of bushing is to achieve a minimum of 40 years [5].

2.3.1 Conductor

One of the primary component in any bushing is conductor that carries rated current and experience the operating voltage which the bushing is designed for. The size of the conductor depends on the rated current that the bushing is designed to carry. There are other two factors that influence the size and material of the conductor are skin depth and the generated power loss because of the current flow in it. Majority of the bushing manufacturers use copper or aluminium for the conductor material. The outer area of conductor carries most of the current and the current flows inside the conductor till the the depth of the material is reached [10]. The power loss generated follows the below equation,

$$P_{\text{losses}} = I^2 \times R = I^2 \times L \times \frac{\rho}{A}$$

I = Rated current of the conductor
L = Length of the conductor
A = Area of the conductor
ρ = Resistivity of the chosen conductor material

From the above equation (need to number), it shows that power losses are inversely proportional to the diameter of the conductor. IEEE/ANSI standard defines the different conductor diameter values for different current ratings. Most bushing manufacturers in the globe refer these standards while selecting the conductor diameter. Larger the conductor diameter, higher the withstand voltage and possess higher PD inception voltage. Besides, Large conductor diameter provides greater ability to withstand larger mechanical forces. Another significant factor to be considered during conductor diameter selection is temperature which is also defined in the relevant standards [10].

2.3.2 Outer Insulation

The type of insulation media and the construction type impacts the selection of length or size of the insulation.The dimension of the insulation should be capable to withstand the operating voltage and over voltages during transient, switching event, lightning etc. For the application that requires two different insulation media on either ends, the insulation length depends on the insulation medium which has lesser dielectric strength. Depends on the application, the insulation media can be Air, Oil, SF_6 [10].

2.3.3 Flange

The purpose of metal flange is to mount the bushing on the equipment where it is installed. The second purpose of the bushing is to contain the gasket. The flange of the bushing that is highly dynamic is usually made of cast aluminium whereas the flange for the lesser dynamic is fabricated from steel or aluminium material. In the case of high current bushings, the flange is made up of aluminium or non-magnetic materials can also be used to cancel out the magnetic losses that is occurred due to the induced current in the flange by the conductor [6] [10].

2.3.4 Oil Reservoir

An oil reservoir is popularly known as expansion cap, which is necessary for higher kV bushings. This serves two main purpose, the first one is to contain the expansion of mineral oil at its elevated temperatures as the mineral oil undergoes expansion and contraction depends on the temperature. Secondly, it is needed to submerge the oil impregnated insulating paper completely to maintain its insulation properties. Therefore, sufficient amount of oil is maintained in the reservoir to keep up the oil over the paper at the lower temperatures. In addition, the oil reservoir is required to contain sufficient gas quantity like nitrogen so that excessive pressure build up can be avoided at higher temperature. This is because the excessive pressure results

in leakage of oil. An Oil-level gauge is usually integrated in the reservoir to ensure sufficient oil level is maintained [6] [10].

2.3.5 Corona Ring

In high voltage components, the geometry of the surface becomes a vital factor in preventing corona discharge. Corona is generally defined as an electrical discharge that occurs due to the ionization of air present around the sharp conductive points like bushing head. The ionization of air is caused by the presence of high localized electric field gradient and it is a luminous, audible discharge, producing a hissing sound. The function of corona ring that can be found in any high voltage equipment is to suppress corona discharge. By designing a spherical shaped corona rings or toroid or shields of larger diameter and manufacturing it to have smooth polished surface greatly control the electric field so that it prevents the corona discharge to occur.The diameter of corona ring increases with increase in operating voltage of the installed equipment. In HV bushings, the corona ring is made of aluminium material and it evenly distributes the potential around the top terminal so that there is no potential difference across the various parts of the ring [16].

2.3.6 Test Tap and Voltage Tap

2.3.6.1 Test Tap

According to IEC 60137, the test tap is defined as the connection that is insulated from the metal flange.This tap can be accessible from outside of the bushing and connected to the outermost foil of the capacitance graded bushing type. The test tap facilitates the measurements of DF, capacitance and PD while the flange is grounded [8].

2.3.6.2 Voltage Tap

According to IEC 60137, the voltage tap is defined as the connection that is insulated from the metal flange. This tap can be accessible from outside of the bushing and connected to the second outermost foil of the capacitance graded bushing type. The voltage tap acts as voltage source for the external power equipment while the bushing is in operation, and also facilitates the measurements of DF, capacitance and PD [8].

2.4 Methods for monitoring bushing insulation - Onsite

Bushings are manufactured in such a way it provides required mechanical support and be capable of withstanding high operational stresses, large current in conductor and experience high temperature during its operation. Besides, in most of the applications, bushings are exposed to harsh environmental conditions. It can also be prone to damage during transportation and installation at the site. Hence, it is

important to monitor the condition of bushing onsite to ensure its normal operation during its lifetime. This helps to detect any fault at its initial stage thus preventing the bushing failure and in turn the transformer outage, which is very expensive [21]. There are few diagnostic methods that are carried at onsite to monitor the healthiness of the bushings are listed below

1. Line Frequency Power Factor (PF) Testing
2. Dielectric Frequency Response (DFR)
3. PD Monitoring
4. Online Monitoring System

2.4.1 Line Frequency Power Factor (LFPF) Testing

The term *Power Factor* is defined as the ratio of the power dissipated in the insulation to the product of effective voltage and current when the bushing is tested with sinusoidal rms voltage at the given conditions. In other words, it is also known as PF for insulation and can also be defined as the cosine of the phase angle between the voltage and resultant current in case of both voltage and current are sinusoidal. Power factor for the insulation is popularly known as Dissipation Factor (DF) or tangent delta though it is calculated in different ways. The DF will be explained in detail in the 2.5.1. As shown in the Figure 2.6, C1 is the main or primary capacitance is the capacitance between the first foil and the test tap or between the first foil and the voltage tap. The tap configurations are explained in the section 2.3.6. The C2 capacitance as shown in the Figure 2.6, it represents the capacitance between the test tap without tap cover and the grounded flange. The C2 for bushings with voltage tap represents the capacitance between the second outermost and the outermost foil.
This offline testing technique is usually done at 10 kV and the measured dielectric losses in the insulation is represented in %. If there is any deviation from the limit stated in the standards, it shows that some kind of degradation may present in the bushing insulation that caused abnormality in the PF and Capacitance values [21]. The standard IEEE C57.19.01 defines the guidelines for the interpretation and verification of Pf test results [7] and the standard IEC 60137 defines the dimensions and performance characteristics for bushings installed outdoors [8].

2.4.2 Dielectric Frequency Response (DFR)

As already mentioned in the section 2.2.2.2, the insulation system of RIP bushings electrically behaves a capacitors connected in series. DFR response, an offline and non-destructive testing technique indicates the condition of composite insulation system that varies with frequencies. This test measures the healthiness of the insulation system over the wide range of frequencies which provides useful information rather than conducting the test at line frequency during PF test or at the narrow band of frequencies during Narrow Band DFR testing method.
DFR method is an in-depth evaluation of bushing insulation, and the significant information can be inferred from the DFR response, such as moisture content retained in the paper and the conductivity of oil in case of OIP bushing type, which

is discussed in the section 2.5. Additionally, the measurements at lower frequencies provide knowledge about any physical defects or the presence of contaminants that reduce the dielectric strength. DFR equipment uses 140 V for testing. However, electrical noise causes an accuracy problem due to lower currents, and the test is conducted over a wider range of frequencies. This can be improved by using voltage amplifier in connection with DFR equipment to cancel out the noise so that the customer gets more reliable and accurate measurements [21]. The standard IEEE C57.12.200 defines the guidelines for performing the DFR test at the factory or at the site and also the present how to interpret the results based on the comparison [9].

The thesis project focuses on DFR simulations of Transformer bushing and how extensively the DFR is useful to detect the potential defects in the bushings. The detailed background behind DFR is presented in the section 2.5.

2.4.3 PD Monitoring

The standard IEC 60270 defines the guidelines for conducting PD measurements for transformers or bushings at the factory/offline testing/re-testing at the factory/online monitoring. During PD assessment, a bushing tap is used, and the main capacitance C1 behaves as a coupling capacitor to acquire PD measurements. However, the PD measurements are sensitive to the external factors, and this can be prevented by proper screening during the testing at the factory. On the other hand, the onsite PD evaluation are greatly disturbed by the external discharges that occur in transmission lines or bushing surfaces in the range of some nano-coulombs and the coronal discharges can even the screen the actual PD events from transformers or bushings [23].

Therefore, the PD response from online monitoring is not reliable while assessing the bushing condition evaluation. Nevertheless, the Ultra High Frequency Sensor in transformers which is installed in close proximity ot the bushings can capture PD inception in the bushings.On the whole, the DF and capacitance values are more reliable in determining the condition of bushing insulation.

2.4.4 Online Monitoring System

A few online monitoring tests can only be done periodically since the accessibility to bushings in service is limited. For example, infrared scan is used to locate high temperature stress due to bad contacts, overloading ; ultraviolet cameras or acoustic techniques or imaging are used to detect corona or surface discharge. However, the most prevalent online monitoring method is to measure capacitance and DF. Depending the installed site and the application, oil pressure and gas analysis are also be done. There are two main benefits that online measurements provides such as monitoring bushing in its operating conditions, and early detection of any degradation in bushing insulation. The main challenge lies in maintaining the reliability of measurements as it is intensively affected by external disturbances [23].

2.5 Dielectric Frequency Response technique

According to the IEEE standard [9], DFR is a offline testing technique and emerged as an significant assessing tool for the insulation system in power system equipments. DFR is defined as the representation of dielectric response in frequency domain. It is also known as Frequency Domain Spectroscopy as the measurements are analyzed over the spectrum of frequencies. The responses are used to evaluate the condition of bushing insulation condition in the field to prevent any unplanned failures or outages in the transformer. Major of the bushing manufacturers conduct DFR at the factory before it is installed at the site. This measurement forms the base reference for a healthy bushing and aids in comparison of the the results which will be obtained when tested during its lifetime. This comparison between the results from Factory Acceptance Test (FAT) and from onsite is valid only under the similar test conditions.
The dielectric response actually outputs the PF and Capacitance as it sweeps over the range of frequencies. The PF curve reflects the dielectric loss characteristics, caused due to the conduction and polarization within insulation. In bushings, it is developing as an important tool to capture the defects at its early stage which may not be detected by other onsite insulation diagnostic methods. It is well proven measuring technique in OIP bushings where as other composite insulation system like RIP , RIS which were discussed in the previous section 2.2.2.2 are still required to extensively prove its reliability in monitoring the bushing hybrid insulation system [9].

2.5.1 Background

DFR is similar to the LFPF testing technique which measures the PF and capacitance at specific frequency 50 Hz/ 60 Hz whereas DFR technique measures over the range of frequencies typically from 1kHz to 10 mHz. During measurement, the range of frequency is influenced by the thermal condition of the insulation system and also the interferences by the environmental conditions. Hence, it requires more understanding to choose the optimal range of frequency for different conditions. The dynamic condition of bushing insulation is well inferred from the change in DFR curves from its reference values and some defects affects PF values to greater extent at lower frequencies which cannot be observed at line frequency.
The transformer bushings of RIP condenser core type consist of insulation system that is represented by parallel plate capacitors connected in series. For such a parallel-type capacitor, the capacitance with vacuum in between is given as

$$C = \frac{\varepsilon_0 \times S}{d} \tag{2.1}$$

where:

- C is the capacitance of the parallel plate capacitor (F)
- ε_0 is the vacuum permittivity ($\approx 8.854 \times 10^{-12}$ F/m)
- S is the area of the plates (m^2)
- d is the separation between the plates (m)

Instead of vacuum, there exists an dielectric material having relative permittivity ε_r, then the capacitance is given by the following equation 2.2,

$$C = \frac{\varepsilon_0 \times \varepsilon_r \times S}{d} \tag{2.2}$$

where:

- ε_r is the relative permittivity (dimensionless)

$$\varepsilon_r = \frac{\varepsilon}{\varepsilon_0} \tag{2.3}$$

where:

- ε is the absolute permittivity of the material (in F/m)

From the above equation 2.2, it can be clearly seen that capacitance varies with frequency and aging. Relative Permittivity of few insulating material are presented below in table 2.1 for an overview. During measurement, the change in capacitance from the standard name plate value is observed as as sign of some defect in the bushing.

Material	**Relative Permittivity**
Air or Vacuum	1
Mineral Oil	2.2
Water	80
OIP or RIP	2–4

Table 2.1: Relative Permittivities of Common Insulating Materials

The composite insulation is ideally a pure capacitor and in real time, losses can occur when the dielectric is influenced by electric field. This field is caused due to the conduction and the movement of electric dipoles formed within the material. Dielectric loss represents the rate of conversion of electrical energy to heat and it exhibits the condition of insulation material.When the dielectric is applied with external voltage, the capacitive current I_C starts flowing which leads the external voltage by 90°. The resistive current I_R starts flowing in phase with the voltage applied due to the dielectric loss that occurs within the material. The basic circuit representation of the insulating material is shown in the Figure 2.7.
The capacitive current I_C is given by the equation 2.4

$$I_C = V \times \omega \times C = 2\pi f \times C \times V \tag{2.4}$$

where:

- V is the external applied voltage (in V)
- f is the frequency (in Hz)

The magnitude of I_R components is usually very small for the good dielectric system when compared to I_C in the bushings. However, the I_R value becomes prominent when the insulation system experiences aging, contamination due to dirt and dust, ingression of moisture, higher oil conductivity, formation of carbonized path etc.

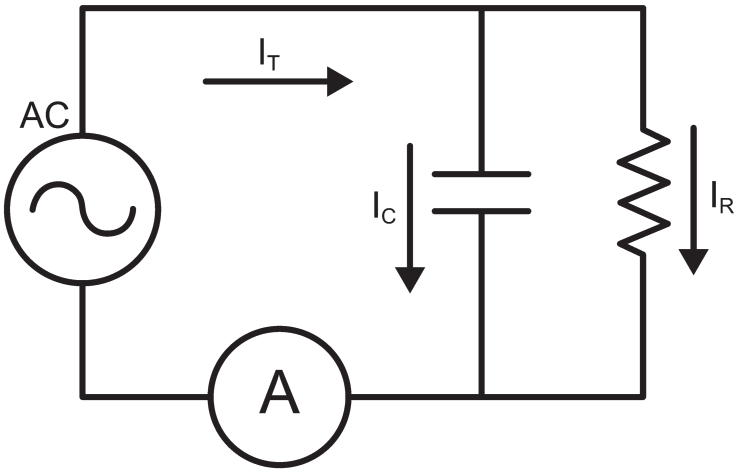

Figure 2.7: Electrical Circuit representation of Insulating material [9]

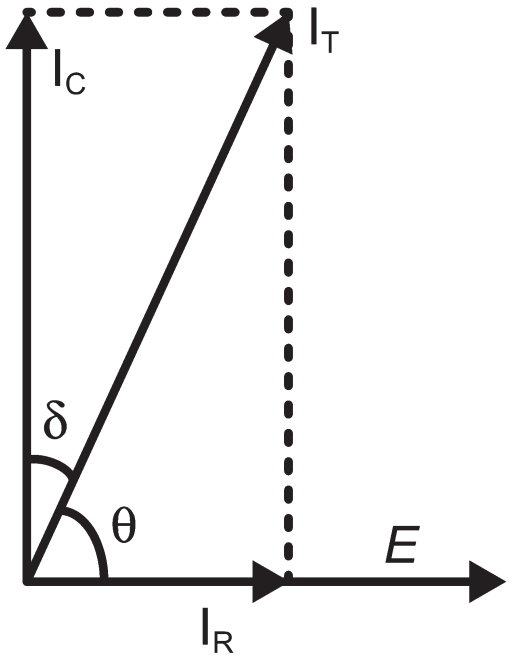

Figure 2.8: Phasor Representation of PF and DF [9]

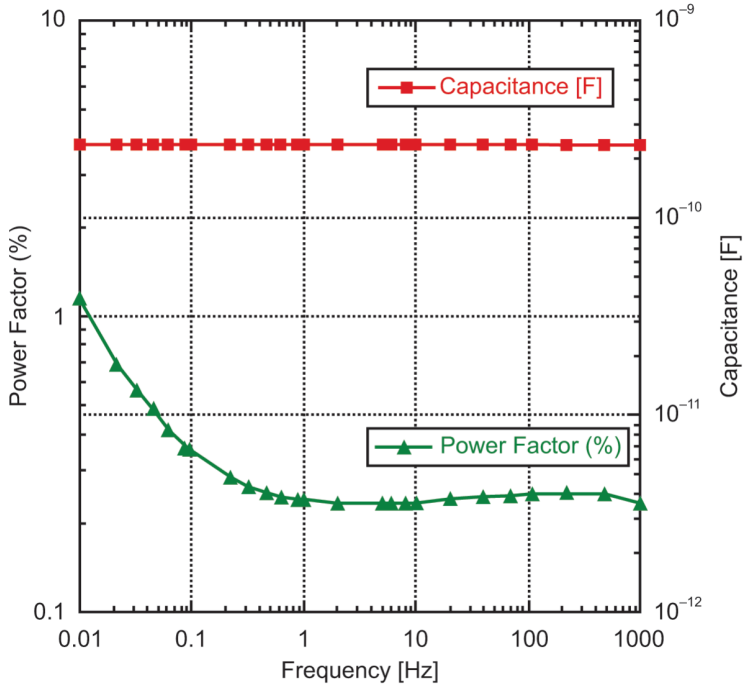

Figure 2.9: Typical DFR response of an OIP bushing [9]

From the above phasor diagram 2.8, the PF and DF expressions are formulated as given in the equations 2.5, 2.6.

$$\cos\theta = \frac{I_R}{I_T} \tag{2.5}$$

$$\tan\delta = \frac{I_R}{I_C} \tag{2.6}$$

where

$$\delta = (90° - \theta) \tag{2.7}$$

By performing the LFPF testing at single frequency or DFR, over the range of frequencies, it outputs the DF, PF and capacitance values the aids in assessing the insulation system condition. The magnitudes of PF and DF are very close if the value of δ is less than 5 °.

2.5.2 Measurement of DFR on Bushings

2.5.2.1 Interpretation of typical DFR response

The response from the DFR measurements is usually the graphical representation of PF and Capacitance values in y-axis plotted against the frequency scale in x-axis, as depicted in the Figure 2.9. It is preferred to represent the values in logarithmic scale on both the x and y - axes for better illustration of the complete DFR measurements. From the Figure 2.9, it can be seen that capacitance curve shows minimal variation when compared to the PF response measured over the chosen frequency

range.

The experimental setup and testing procedure of the DFR is similar to the PF testing at power frequenct as specified in the standard IEEE Std 62 ™-1995. However, the only difference is the PF testing is performed at line frequency whereas the DFR is measured for the range of frequencies. The condition of bushing insulation is well captured when it is tested the over the range of frequencies. From the PF curve pattern and magnitude as shown in the Figure 2.9, it tells if there is any potential defects or developing deterioration inside the insulation system. The DFR testing is performed in the bushings using test tap or voltage tap. The effect of deterioration in the insulation system is more pronounced in the lower frequency range which can be well observed from the DFR response [9].

2.5.2.2 Analysis of DFR Results

When compared to LFPF testing, DFR brings added information about the quality of the bushing insulation. In principle, the change in capacitance exhibits the defect in the mechanical structure of the bushing such as shorting of foils layers in the core and the DF is the indication of quality of the insulation. In the majority of the tests, the magnitude of capacitance and DF at line frequency are identical in DFR and 10 kV LFPF testing. The bushing is further taken into investigation when the tester is not obtaining the identical values.
The analysis of DFR is based on the comparison with reference values which is obtained from the manufacturer stated during the testing at factory or from previous routine test. This type of comparison is termed as time based comparison. In this thesis project, the DFR results are obtained through COMSOL simulation is compared with the reference DFR experimental data of healthy bushing. DFR measurements are greatly influenced by the external factors such as humidity, temperature and position of mounting and therefore the comparison with the base line data and test data should be done under same test condition to obtain reliable data interpretation. Hence the results which are taken onsite at different operating temperatures of the bushings should be corrected to reference temperature of 20° before the results analysis. This conversion is called Individual Temperature Correction (ITC) using Arrhenius Theory. The temperature dependence of dielectric materials and to perform the temperature correction in the DFR measurements can be modeled according to the Arrhenius equation as given in 2.8.The capacitance and PF curves shows no prominent change if the insulation system functions in proper condition given there is no change in mounting situation.

$$L = \ln f_2 - \ln f_1 = -\frac{E_a}{k_B}\left(\frac{1}{T_2} - \frac{1}{T_1}\right) \tag{2.8}$$

where:

- E_a is the activation energy of the insulation material(eV),
- k_B is the Boltzmann constant, $k_B = 8.167 \times 10^{-5}$,
- T is the absolute temperature (K).

In the Figure 2.10(a), the red curve corresponds to measurements at 24°C and the green curve that corresponds to green curve 16°C is the reference data for compar-

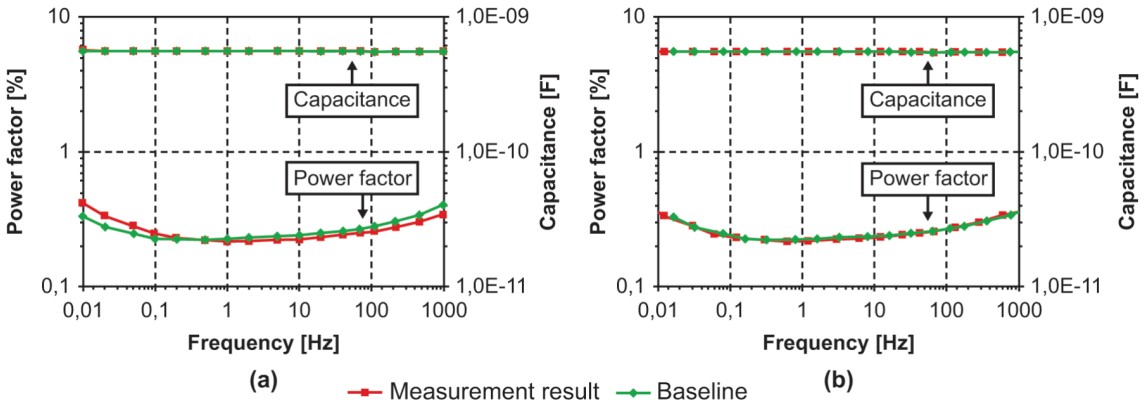

Figure 2.10: DFR Measurements of RIS Transformer Bushing (a) Before Temperature Correction (b)After Temperature Correction [9]

ison. The Figure 2.10(b) shows the response after the measurements reference to 20°C which completely overlaps with the baseline data. This depicts the significance of temperature correction in the DFR measurement data.

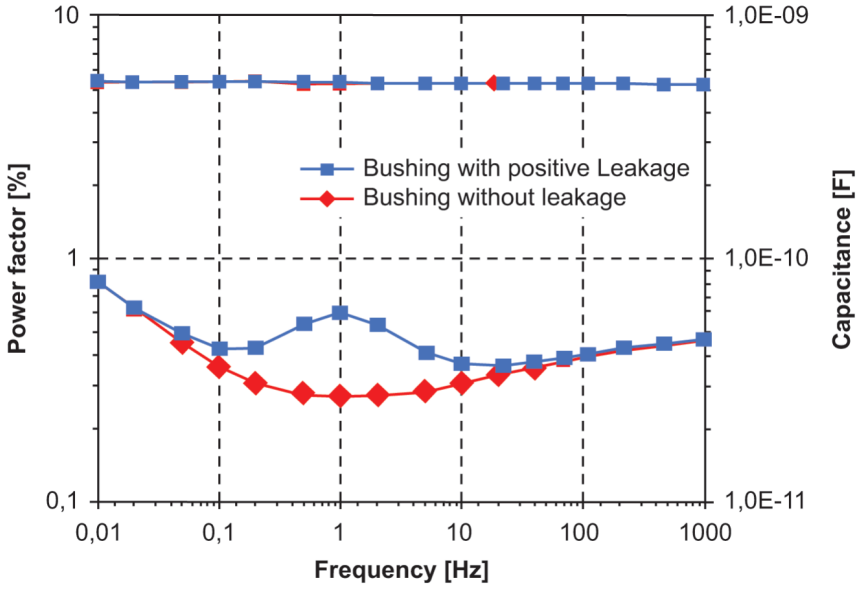

Figure 2.11: DFR Response of Good Bushing(Red curve) and the Defective Bushing(Blue curve) [9]

The Figure 2.11 shows the DFR measurement of good OIP bushing (red curve) and the defective bushing (blue curve) which has distorted PF value of having a bump at 1 Hz. This implies that the distorted PF curve is due to the some abnormality in the bushing. The defect identified is due the flow of crepe current in the air side of the tested OIP bushing. Thus the DFR is efficient in capturing the defects in the bushing. However, the challenge in DFR response analysis is to predict the exact root cause that brings the the abnormal DFR trend [9].

2.6 Modelling with COMSOL Multiphysics

To solve the multiphysics, fluid and structural problems, Finite Element Methods (FEM) are broadly used since many years. It facilitates engineers in various domain to build the complex models mathematically and solve using numerical problems. Modeling and solving using FEM helps to evaluate design and performance for the developed model in the realistic environments. This results in bringing up the safe, reliable and cost-effective design which makes the product functionality to withstand any unprecedented circumstances [24].
COMSOL Multiphysics is one such software that uses Finite Element Method for the computation of the developed model. It is a simulation interface to build and simulate the fully coupled multiphysics and single physics assigned models [25]. In COMSOL, Model Builder encompasses all the steps in modeling process flow that includes

1. Defining geometries
2. Assigning materials to the developed geometry and define require material parameters
3. Assigning physics to the geometry
4. Building good quality mesh
5. Defining the desired study for computation
6. solver configuration
7. Visualization and result evaluation

Modeling of a design, product or process using multiphysics results in optimizing the process and bringing up more efficient and accurate design. In this project, transformer bushing is modeled in the model builder and then by adding the appropriate boundary conditions, meshing and the frequency domain study will be chosen to perform the frequency sweep over the desired range. In the results, capacitance and tan δ as a function of frequency will be obtained which will be discussed in the upcoming chapter 4 [25].

2.6.1 Electrostatics

The "Electrostatic" interface is available under Electric Fields and Currents of AC/DC module in COMSOL Multiphysics. By using this interface, the user can compute the problems related to electric field, electric field displacement and potential distribution when the electric charge distribution is assigned explicitly. The analysis involved is stationary formulation. Basically, it solves electric field problem using the Gauss's law by having potential as its dependent variable. The required boundary conditions must be added to compute the desired analysis precisely which will be explained comprehensively in the section 3.1.3.1. The COMSOL computes the following two equations 2.9, 2.10 to study the electric field and the electric field displacement in the model [26].

$$\nabla \cdot \mathbf{D} = \rho_v \tag{2.9}$$

$$\mathbf{E} = -\nabla V \tag{2.10}$$

where

- **D** is Electric Displacement Density
- ρ_v is Volume Charge Density
- **E** is Electric Field
- V is Electric Potential

The transformer bushing model developed in this project is assigned with electrostatic physics to analyze how the defects in the bushing condenser core and the outer parts affects the uniform electric field distribution at the defective location and to what extent the defect is captured in the evaluation of capacitance and DF using this formulation.

2.6.2 Electric Currents

The "Electric Current" interface is available under Electric Fields and Currents of AC/DC module in COMSOL Multiphysics. By using this interface, the user can compute the problems related to electric field, electric current and electric potential distribution in the conductive media where the inductive effects are negligible. It solves current conservation equation according to Ohm's law by having potential as its dependent variable. This interface is well suited for modeling good conductors where Ohm's law is applicable but not for bad conductors like air and Insulators. The required boundary conditions must be added to compute the desired analysis precisely which will be explained comprehensively in the section **??**. The COMSOL computes the following three equations 2.11, 2.12, 2.13 to study the electric field and the electric current in the model [27].

$$\nabla \cdot \mathbf{J} = 0 \tag{2.11}$$

$$\mathbf{J} = \sigma \mathbf{E} + \mathbf{J}_e \tag{2.12}$$

$$\mathbf{E} = -\nabla V \tag{2.13}$$

Where

- **J** is the Current Density
- σ is the Electrical Conductivity
- **E** is the Electric Field
- $\mathbf{J}_e$ is the External Current Density
- V is the Electric Potential

The transformer bushing model developed in this project consists of core with conductive foils within the insulating paper. Therefore, it is assigned with electric current physics to analyze how the defects in the bushing condenser core and the outer parts excluding the installed environmental conditions affects the charge density, electric field & electric potential at the defective location and to what extent the defect is captured in the evaluation of capacitance and DF using this interface.

2.7 Dielectric Response Measurements

There are many companies that offer wide range of frequency response analyzers to perform DFR measurements and few are listed as follows, FDS-PDC Frequency Response Analyser from Goldsol, [28] DIRANA - Dielectric Frequency Response Analyzer from Omicron, [29] and the popular from Megger - IDAX series of insulation diagnostics analyzers. [30] The DFR measurements that is considered for this work as reference measurements was taken by using Megger IDAX 300 as presented in the Figure 2.12.

Figure 2.12: Insulation Diagnostic Analyzer - IDAX 300 [30]

2.7.1 Megger IDAX Insulation Diagnostic System

Megger offers wide range of insulation diagnostic analyzers under IDAX series. By adapting these range of instruments, DFR measurements can be done at the field or at the factory. As mentioned in the previous section 2.5.1, DFR response is the measurement of DF and Capacitance over the frequency range. IDAX is used to measure the moisture ingress in the solid insulation and the conductivity of oil at the reference temperature of 25°C and DF at 20°C reference. These instruments internally use ITC to perform temperature correction in the DFR test data. The IDAX instruments is integrated with a computer to ease the post processing of measurements after testing and the user interface of the IDAX software is presented in the Figure 2.13. This software is also designed with ITC especially to assess the insulation condition of bushings and instrument transformers. The benefits of IDAX software are easy to use, automated test-flow and representation of results that are easily understandable. DFR testing by IDAX measurements are compatible to the international standards and guides that includes CIGRE TB 254, CIGRE TB 414, CIGRE TB 445, CIGRE TB 775, IEEE C57.152-2013, IEEE C57.161-2018 [30].

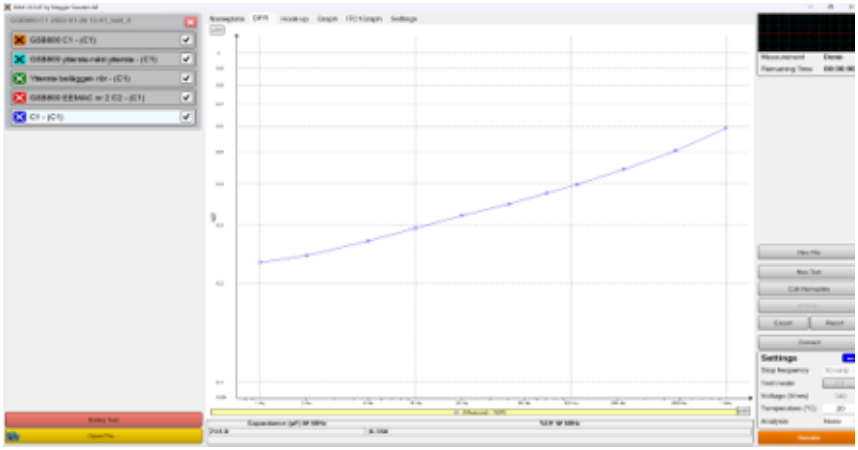

Figure 2.13: Representation of DFR data in the IDAX software

3

Dielectric Response Modeling and Measurements

3.1 Condenser Bushing Model

To perform DFR simulations of transformer bushings, it is important to model the bushing in a way that the model should reflect the bushing geometry in real time. This in turn also aids in obtaining the results from simulations which are more reliable and can be taken as base for further investigations. In view of this context, the transformer bushing of type GSB 800 OA is modeled using COMSOL Multiphysics and eventually the required computations to obtain DF and capacitance are carried out. The following sections explain the process flow in obtaining the 2D Antisymmetric model of the chosen bushing in a detailed way. The Figure 3.1 shows that 2D revolved geometry of the bushing developed in COMSOL.

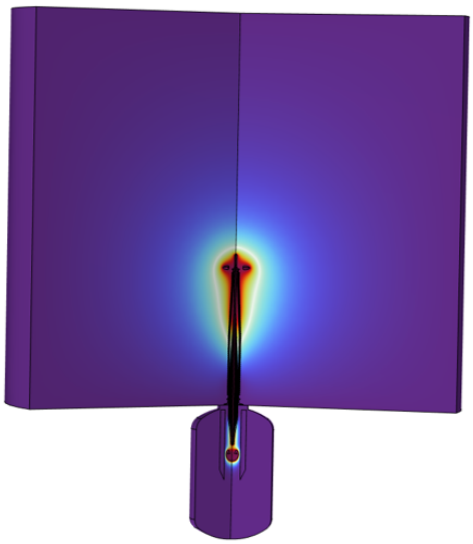

Figure 3.1: 2D Revolved Geometry of Transformer Bushing

3.1.1 Implementation of Geometry in a Test Room

The transformer bushing geometry is built in COMSOL using Model Builder feature. It provides an easy to follow procedure from building the geometry to obtaining the

results and the consecutive steps are explained in the section 2.6 and presented in the Figure 3.2.The primary goal is to construct the bushing model in such a way it reflects the bushing geometry in real time. This aids in performing the DFR simulations precisely and improves the reliability of the results to compare with the real time DFR measurements.

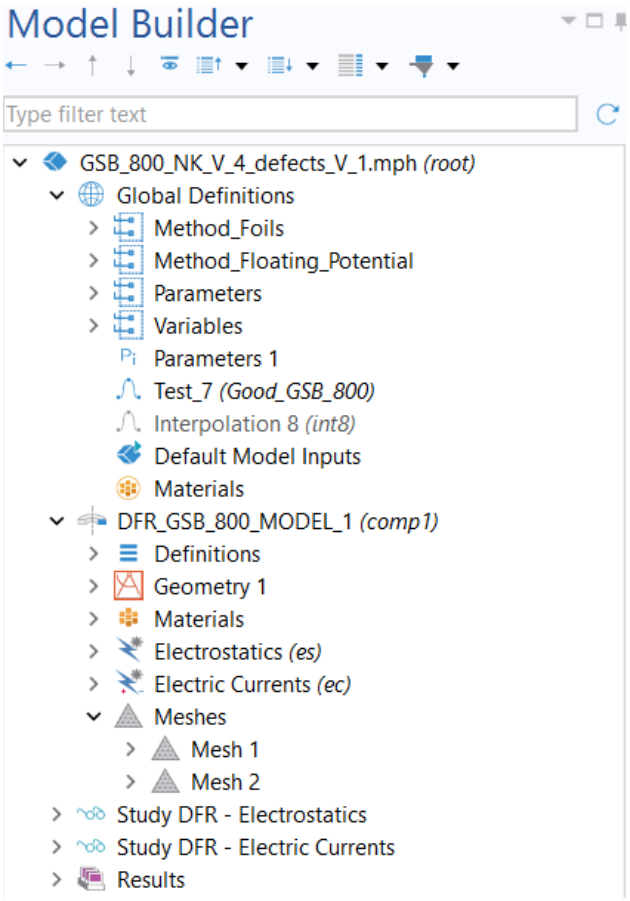

Figure 3.2: Model Builder Tree

The transformer bushing consists of air side and oil side. The air side length is greater than oil side and the bushing part above the flange is exposed to atmospheric air in real time condition. The oil side length is shorter and the bushing part below the flange is immersed in oil tank of the transformer. The bushing model that is developed in this work is 2D Axisymmetric model. As the 2D bushing model is symmetrical about Z-axis, it is sufficient to develop 2D axisymmetric model. To construct the transformer bushing model, a structured approach is followed that starts from building the condenser core, Gel layer , outer Insulator layer, Outer Insulator sheds, flange, corona ring, Oil side shield, test room of air and oil tank with press board. Then the constructed model is assigned with materials, necessary physics, proper meshing to replicate the real time bushing behavior but with the help of simulations. The following sections present the steps involved in developing the bushing geometry in the model builder.

3.1.1.1 Insulation body and metallic foils

The construction of condenser core comprises of central conductor, conductive foils and RIP Insulation. In this thesis project, the first and foremost step is the creation of central conductor and the conductive foils to form capacitance grading. This is achieved effectively by using the Application Builder feature in COMSOL and an overview of Application Builder tree is shown in the Figure 3.3.

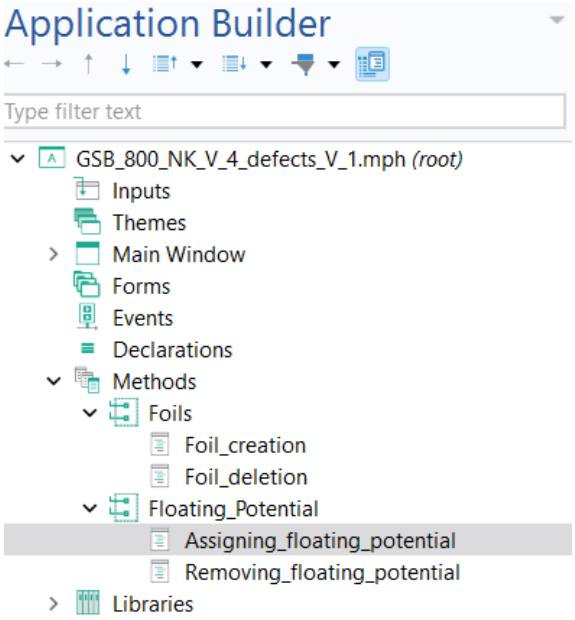

Figure 3.3: Application Builder Window in COMSOL

The method editor in application builder, as depicted in the Figure 3.4, allows the user to write the code which is known as method in JAVA Script to construct the desired geometry and perform any desired action. The methods needs to be called under the *GLOBAL DEFINITIONS* in model builder tree for its execution accordingly. The advantage of using this feature is to save time and effort in performing the repetitive actions. In here, the method editor is used to build foils and assigning floating potential to the foils which is discussed in the section 3.1.3.3. The method or code for creation and deletion of foils is attached in the appendix sections A.1 and A.2 .

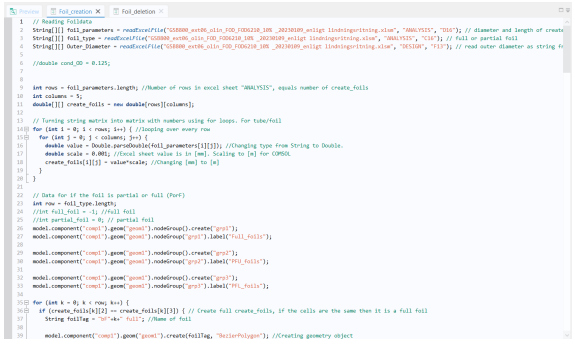

Figure 3.4: Application builder - Method Editor

The execution of method starts from reading an excel file that contains the winding drawing data for GSB 800 OA bushing model. To create the foils in the condenser core, the method reads outer diameter from "DESIGN" sheet and foil data under *ANALYSIS* sheet of the fetched excel file. The foil data under *ANALYSIS* sheet contains the number of foils, type of foil, whether it is partial or full foil, the upper & lower edge of upper partial foils, and the upper & lower edges of lower partial foils. To determine the number of foils to be created, the code read the FOIL NUMBER column and to identify the type of foil, the code compares the lower edge of upper partial foils and the upper edge of lower partial foils. If the values are same, then it is full foil otherwise it is partial foil. After identifying the foil type, the corresponding code to build the foil geometry is executed. In the same fashion, the code runs in a loop until the required number of foils has been created. Along with the creation of foil geometry, the cumulative selection is also added to each created foil to ease the assigning of boundary conditions under physics. The Figure 3.5 shows the geometry of foils after the execution of the method "CREATION OF FOILS".

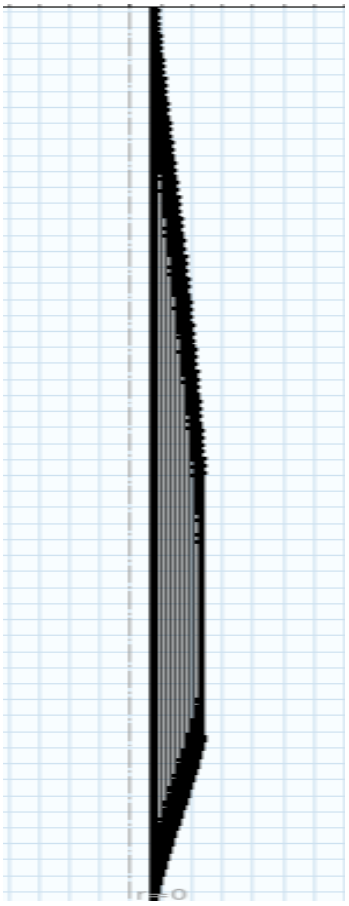

Figure 3.5: Creation of Foil Geometry

The next step is to create the lines between the created full and partial foils to transform into a closed geometry.The lines that are drawn between the created foils to transform in to closed geometry as shown in the Figures 3.6a and 3.6b.The *deletion of foils* is also written to perform the deletion of foils.
After creating the foils, the CAD file for the GSB 800 is imported using *IMPORT*

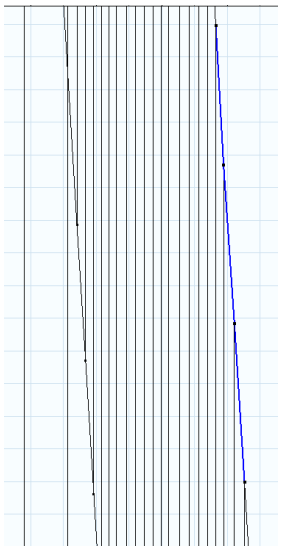

(a) Representation of Lines in Upper Partial Foils

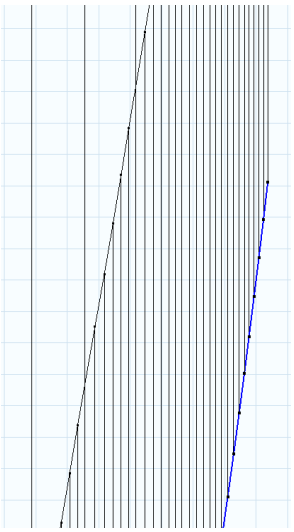

(b) Representation of Lines in Lower Partial Foils

Figure 3.6: Formation of Closed Foil Geometry

option under *GEOMETRY* node. The imported CAD file contains the geometry for conductor, RIP insulation body, Gel layer and the outer insulation sheds. The imported CAD file is shown in the Figure 3.7.

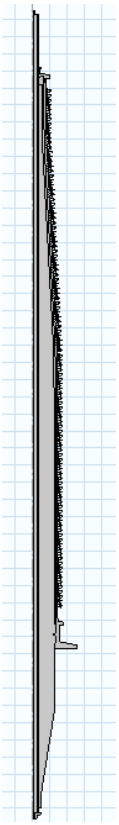

Figure 3.7: CAD Geometry of Transformer Bushing

3.1.1.2 Creation of Outer Geometry

With the constructed RIP core and the sheds, there are other geometries that are needed to obtain the complete model of the geometry. In the imported CAD file, the outer insulator layer is not present hence it is drawn manually having around 5mm distance from Outer shed. The action is performed by using *SKETCH* option in the main ribbon of model builder window. The outer insulation later that is drawn manually is shown in the Figure 3.8.

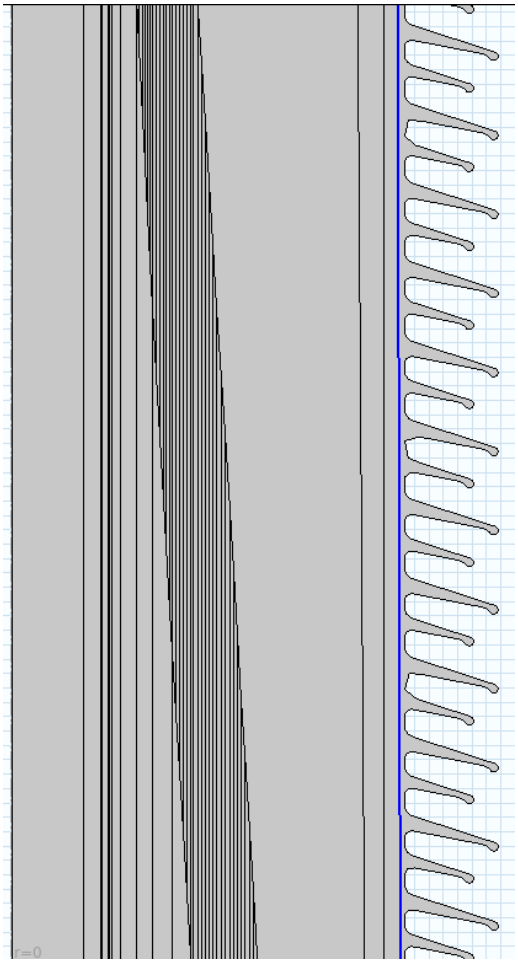

Figure 3.8: Creation of Outer Insulation Layer

The next step is to create the test room for the air and oil side of the transformer bushing and the corona ring. The test room and the corona ring are presented in the Figure 3.9. It is drawn adjacent to the top terminal to evenly distribute the electric potential around the bushing head. The creation of a test room is done by importing a CAD file using the *IMPORT* option as mentioned earlier. Further, there are few more geometrical modifications need to be carried out to split the single boundary into multiple boundaries for the simulation purpose. The COMSOL Multiphysics builds the geometry from top-down and finally, the *UNION* node forms the union of all the objects that are contained in the sequence.

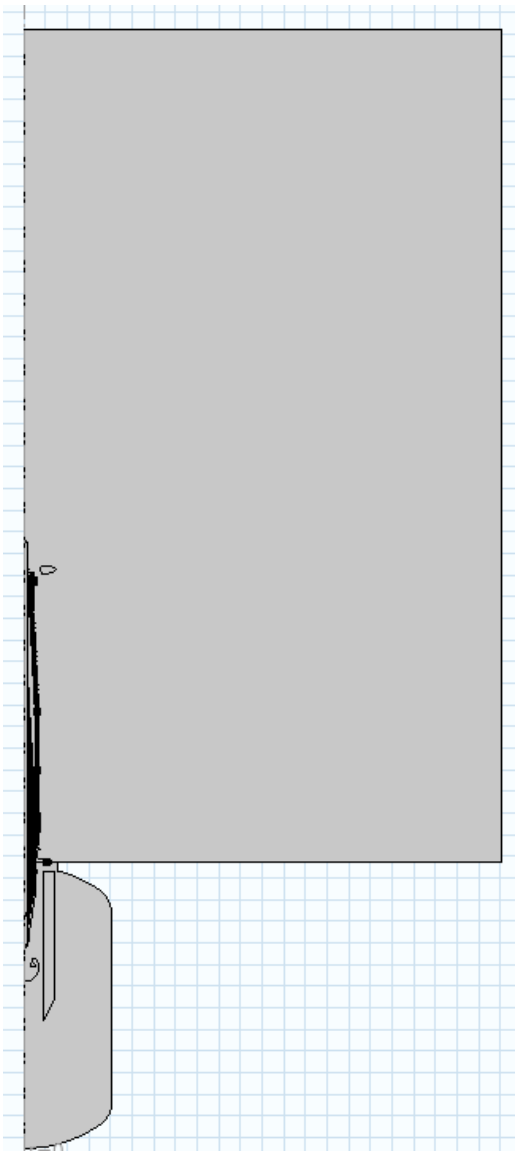

Figure 3.9: Construction of Test Room and Corona Ring

3.1.2 Materials

The next step is to assign the material for each domain in the developed geometry under the *MATERIAL* node in *COMPONENT*. It defines the physical properties with a check mark that is necessary for the assigned physics to compute the model accurately. It is important to assign the correct material to the respective domain as it affects the simulation results.
The desired materials are added by right clicking the *MATERIAL* node and select on *ADD MATERIAL* to choose the material for the domains. If the specific material is required which is not available in the COMSOL Multiphysics library, it can be created by using *BLANK MATERIAL* option. The material properties can be imported from another model or defined separately under *VARIABLES* in *GLOBAL DEFINITION*. If the domain requires the material to be added but if it is missing without the material, COMSOL highlights with red indication. This helps the user

to easily identify the domain where the material is not assigned. The Figures 3.10 and 3.11 show an overview of settings window and the domains that require material under *MATERIAL* node.

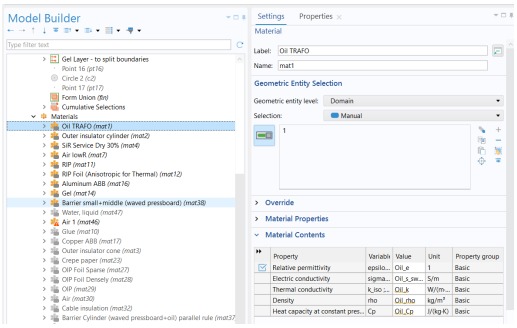

Figure 3.10: Material Setting Window

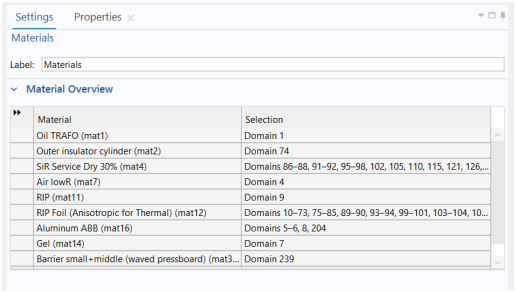

Figure 3.11: An Overview of Material and its Respective Domains

The Figure 3.12 highlights the material assigned to the air side of the test room. Likewise, the materials are assigned to the respective domains, such as metal parts, RIP core and its insulation body, gel layer, outer insulation layer, outer sheds, and oil side respectively.

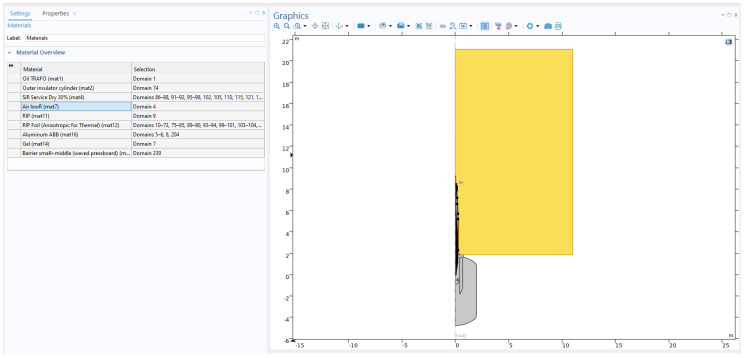

Figure 3.12: Representation of Material Assigned to the Test Room - Airside

3.1.3 Physical Interfaces

To perform the desired computation of the constructed model, it is important to assign the right physics to it. As the DFR is computed only within the condenser

core, it is significant to ensure the condenser core is assigned with right physics for reliable computations. To compute DFR for the developed bushing model, the two physics - Electrostatics and Electric Current are assigned to the respective domains of interest.

3.1.3.1 Electrostatics

The Figure 3.13 represents the domains that are assigned with electrostatic physics. In here, the condenser core and the outer domains in the geometry including the test room of air & oil tank are assigned with electrostatic physics.

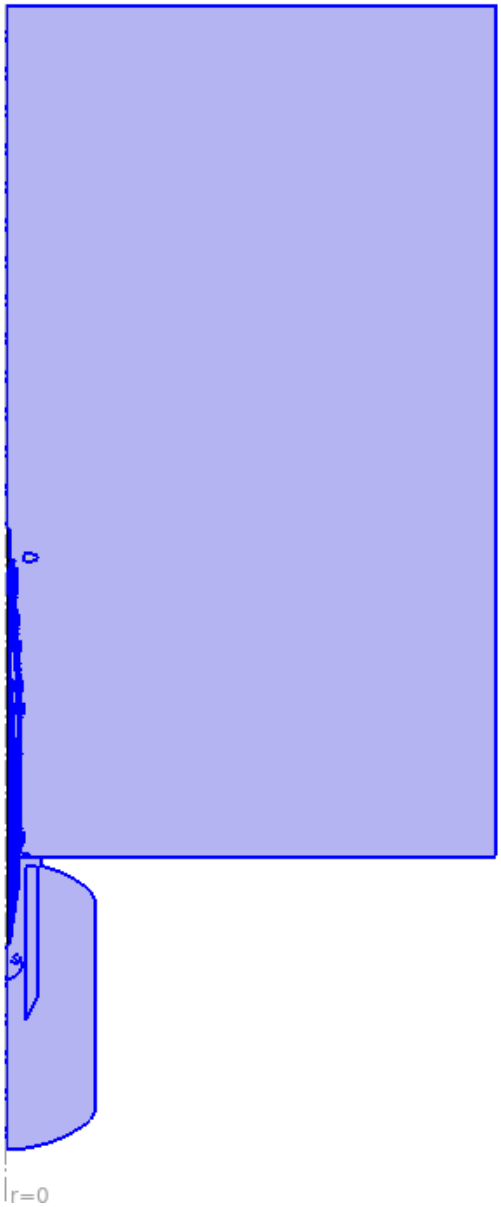

Figure 3.13: Representations of Domains under Electrostatics

3.1.3.2 Electric Currents

The Figure 3.14 represents the domains that are assigned with electric current physics. In here, the condenser core and the outer domains in the geometry, excluding the test room of air & oil tank, are assigned with electric current physics.

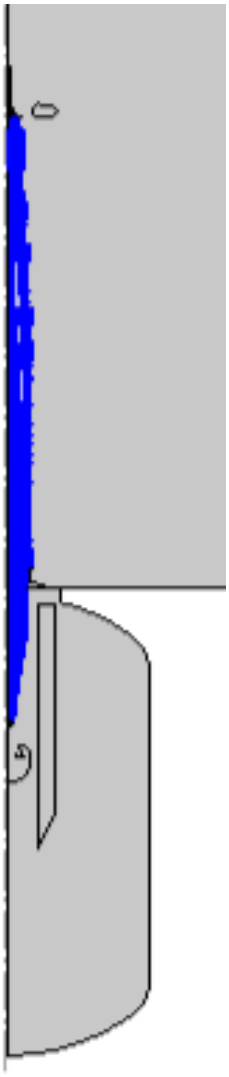

Figure 3.14: Representations of Domains under Electric Currents

3.1.3.3 Boundary Conditions - Electrostatics and Electric currents

While assigning the physics in any model, boundary conditions plays an important role in bringing the behavior of model in real time. The assigned boundary conditions in both the physics are presented below. The Figures 3.15, 3.16, and 3.17 show the boundaries that are assigned with required boundary conditions for both electrostatics and electric current physics. The code for assigning and removing floating potential to the foils are attached in the appendix sections A.3 and A.4.

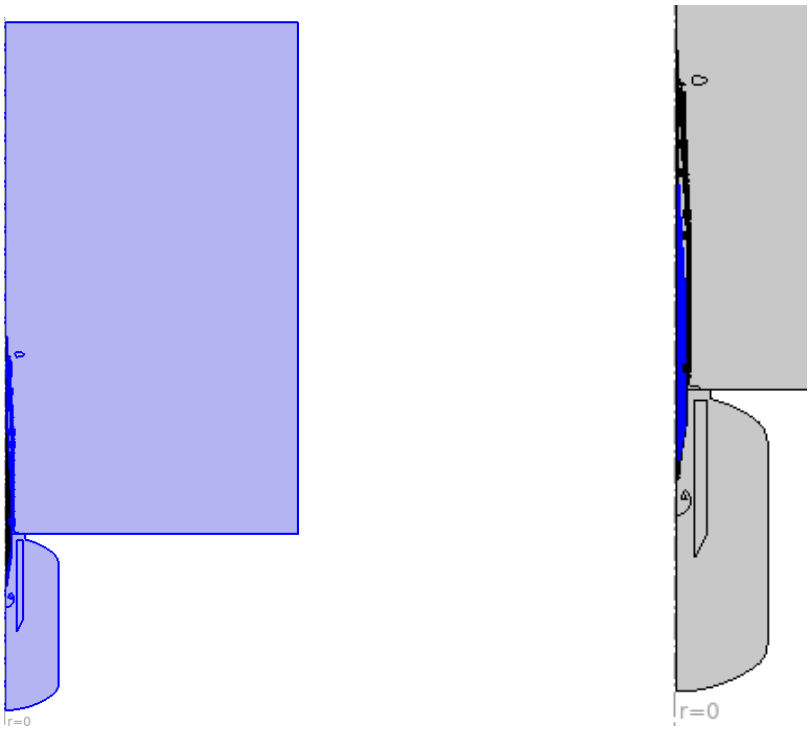

(a) RIP core excluded **(b)** Representation of RIP Losses

Figure 3.15: Charge Conservation

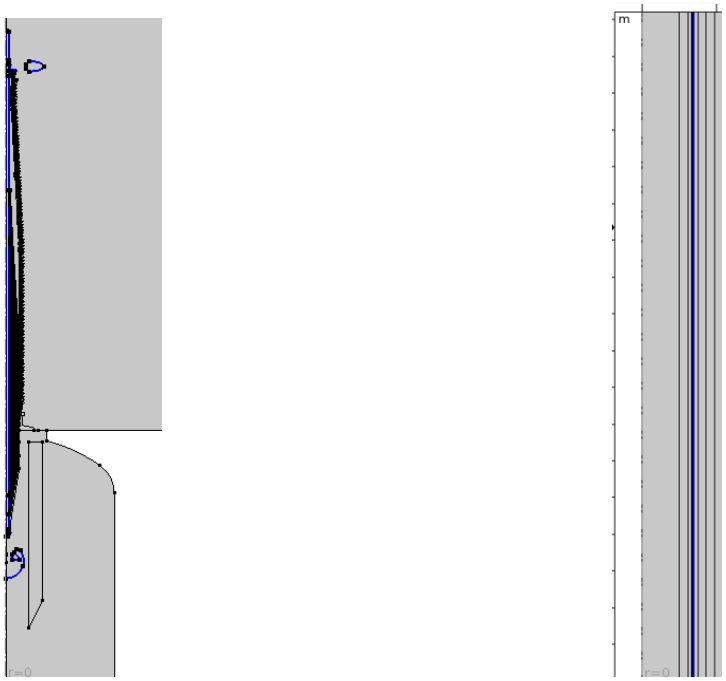

(a) Assigning Potential to Conductors & the First Foil **(b)** Assigning Floating Potential to the Foils

Figure 3.16: Potential and Floating Potential

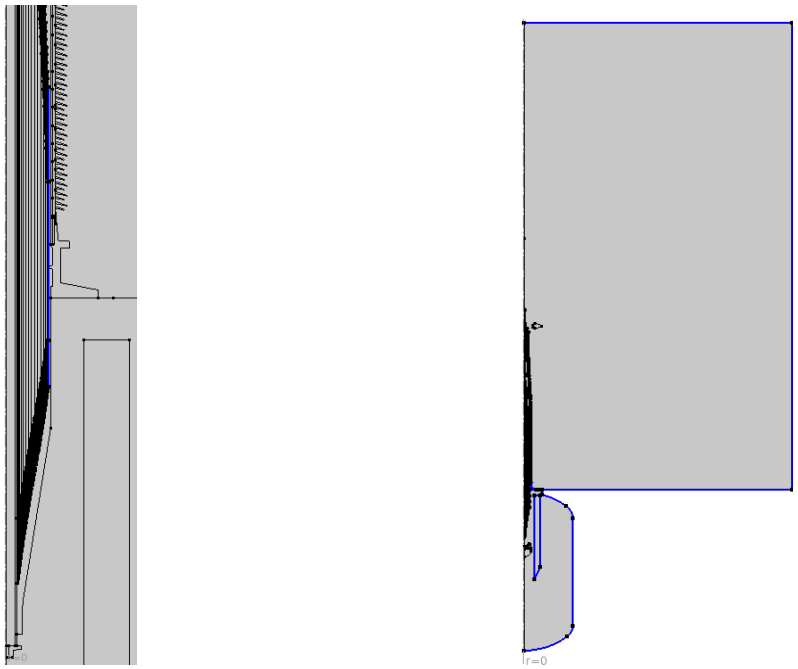

(a) Assigning Ground to the Outermost Foil

(b) Assigning Ground to Flange, Test room & Oil Tank

Figure 3.17: Ground

3.1.4 Mesh

Since COMSOL is FEM based software, the mesh in the geometry is very significant for accurate results. Meshing usually allow discretizations of the domains in the geometry and results in formation of mesh elements. The formed mesh elements are of the similar shape that depends on the mesh type the user provides. There are other properties such as size distribution, size expression and corner refinement also influence the meshing of an entity. Higher the number of discrete elements in the mesh facilitates COMSOL to perform the computations under study in precise way. For the developed bushing model, the triangular mesh is defined at first for the geometry and the resultant triangular mesh in the condenser core is shown in the Figure 3.18.

To generate more discrete points than in the triangular mesh, it is decided to define mapped mesh. Mapped mesh is a type of mesh that forms rectangular mesh elements and each mesh element is formed by joining four points. In this way, it generates more discrete points that helps COMSOL to do accurate computations of the defined study whereas the triangular mesh generates triangular mesh elements by combining three points only. DFR simulations are evaluated in the main condenser core and hence there are extra lines required to draw across the domains of partial foil so that four edges domains are formed. This aids in building the mapped mesh in a proper manner. The resultant mapped mesh is shown in the Figure 3.19.

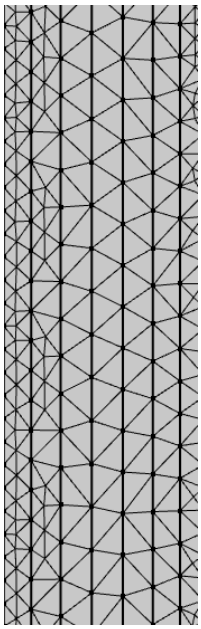

Figure 3.18: Representation of Triangular Mesh

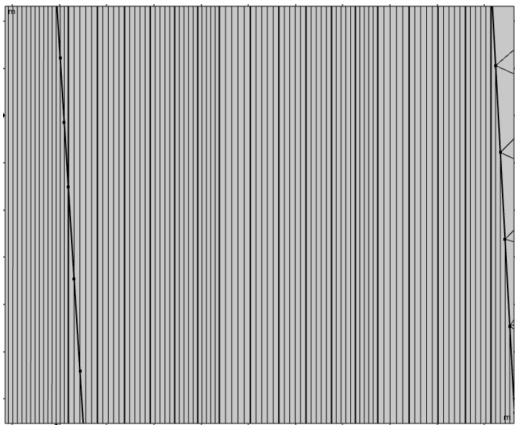

Figure 3.19: Representation of Mapped Mesh

3.1.5 Study - Frequency Domain

The final step in the COMSOL model to perform the desired simulations is to define the correct study type under the node *STUDY*. DFR is nothing but the the representation of dielectric response in frequency domain. The dielectric response represents the dielectric losses that occur within the condenser core of the bushing. Therefore, the frequency domain study is assigned across the range of frequencies as shown in the Figure 3.20. In the study settings, it is important to ensure that the physics and mesh should be chosen correctly to obtain the precise evaluation of DFR. In our mode, two separate study have been defined to study DFR simulations under both electrostatic and electric current physics. It can also be chosen different physics under one study. The purpose to define separate studies is to provide ease in performing simulation for multiple times.

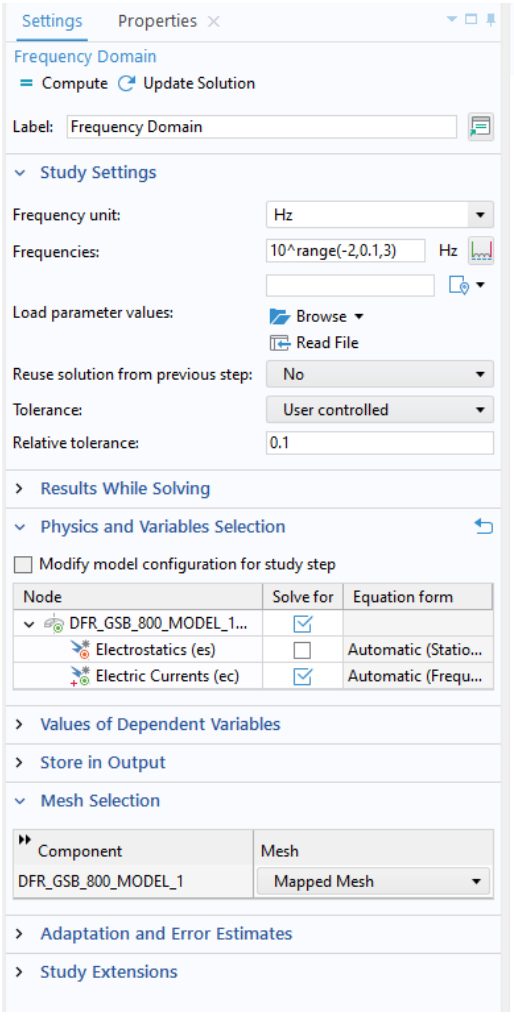

Figure 3.20: An Overview of Settings in Study Node

3.2 Dissipation Factor and Capacitance in COMSOL

In real time DFR measurements, DF and capacitance are evaluated between the HV conductor and outermost foil which is grounded. To reflect this behavior in simulation, two terminals are included as boundary conditions in both the physics as already shown in the Figures 3.16a and 3.17a. The *TERMINAL 1* is assigned to outer boundary of the conductor and the first foil. Terminal 1 is given with voltage of 140 V which is the actual voltage applied from DFR measuring instruments in real time offline testing. The another *TERMINAL 2* is assigned to the outermost foil and is given with ground voltage 0 V. Here tan δ is interpreted via the complex impedance Z which is actually the ratio of imaginary part of impedance to the real part of impedance. This can be well understood in the following equations 3.1, 3.2 and 3.3. In COMSOL, under both the electrostatic and electric current physics, it provides an output variable called terminal admittance Y between the terminals 1 and 2. By availing this terminal admittance variable, the DF is calculated in

COMSOL as the ratio of the ratio of real part of admittance to the imaginary part of admittance by following the fact that the reciprocal of admittance is the impedance. The expression for tan δ in COMSOL is given as per the equation 3.4.

$$Z = Y^{-1} \tag{3.1}$$

$$R = \mathrm{Re}(Z) \tag{3.2}$$

$$X = \mathrm{Im}(Z) \tag{3.3}$$

$$\tan\delta = \frac{\mathrm{Re}(\mathrm{es.Y}_{21})}{\mathrm{Im}(\mathrm{es.Y}_{21})} \tag{3.4}$$

Theoretically, the capacitance is calculated according the equation 3.5 and it is represented in COMSOL using terminal admittance variable as given in the equation 3.6.

$$C = \frac{1}{2\pi f X} \tag{3.5}$$

$$C = \frac{\mathrm{Im}(\mathrm{es.Y}_{21})}{2\pi \cdot \mathrm{freq}} \tag{3.6}$$

For the COMSOL to compute DF and capacitance for the developed bushing model, the expressions 3.4 and 3.6 should be defined using *GLOBAL EVALUATION* under *DERIVED VALUES* in the *RESULT* node of the model builder tree [31].

4

Results

4.1 Implementation of Possible Defects in COMSOL

In many cases of transformer failure, the analysis shows that the bushings were affected as initial faulty component. When bushing in service, it undergoes various kinds of stresses by thermal, mechanical and electrical means.The bushing insulation system is designed in such a way that it must be capable to withstand all the stresses without affecting the normal function of the bushing. These stresses arise due to the occurrence of transient condition during switching events in close proximity in the network, lightning strike or any unexpected failure in other parts of the system. The studies show that the bushings stand as one of the weakest component that contribute to major of the failures in large transformers. The bushing failures are prevented by performing the scheduled maintenance so that the defect can be identified at an early stage and it aids in further investigating the bushing depending on the defect level. This trigger the need for reliable methods for early defect identification so that it eventually cause a cost reduction in maintenance.

Part of the Bushing	**Possible Defect**
Condenser core	Short circuit between conductive layers; Grounding of few outermost conductive layers
Interface between Gel and Outer Insulator	Deposited impurities; Moisture ingress; Change in gel permittivity
External Insulator Sheds	Deposition of salt and pollutants; Contamination due to snow deposition

Table 4.1: List of Defects Implemented in the Bushing COMSOL Model

The table 4.1 presents the typical defects that could occur in the essential parts that play a vital role in ensuring the normal operation of the bushing. The listed defects in the bushing are recreated in the developed COMSOL model using the suitable boundary conditions under the chosen physics to compute the DF and the capacitance accordingly. The significant change in computed DF and capacitance value from the COMSOL calculated values implies that the defect is captured well in the DF response curve. The thesis work further investigates the pattern of loss curve for the defects introduced in the model that helps to predict the type of defect and

the defect level in the bushing. The images were taken from the scrapped bushing that were kept outside the factory for a long period of time.

4.2 Validation of the COMSOL model

After constructing the geometry and assigning the appropriate physics, the next step is to compute the model to perform DFR simulations. As the name DFR implies, the frequency domain study is chosen to simulate loss factor and capacitance values over the chosen frequency range as already mentioned in the section 3.1.5. The frequency range defined in the study is from 10 mHz to 1 kHz with the step size of 0.1 so that the more number of DF values are obtained and plotted against the frequencies in the logarithmic scale for better analysis.

The primary step is to validate the loss factor values obtained from the computed COMSOL model with the real-time DFR measurements to ensure that the developed model provides accurate and reliable simulation results. The loss factor is computed using the equation which is given in the section 3.2. The two study nodes are defined for electrostatic and electric current physics respectively.

The Figures 4.1 and 4.2 show the loss curves obtained from the simulated model using electrostatic and electric current physics and the interpolated real time DFR loss curve values from IDAX software respectively. The irregularities in the obtained frequency dependencies may be due to different causes (e.g., settings for material properties), however, this doesn't affect the general trend. Since the operation frequency is 50 HZ, the values of loss factor and capacitance at this specific frequency is more emphasized in the upcoming sections.

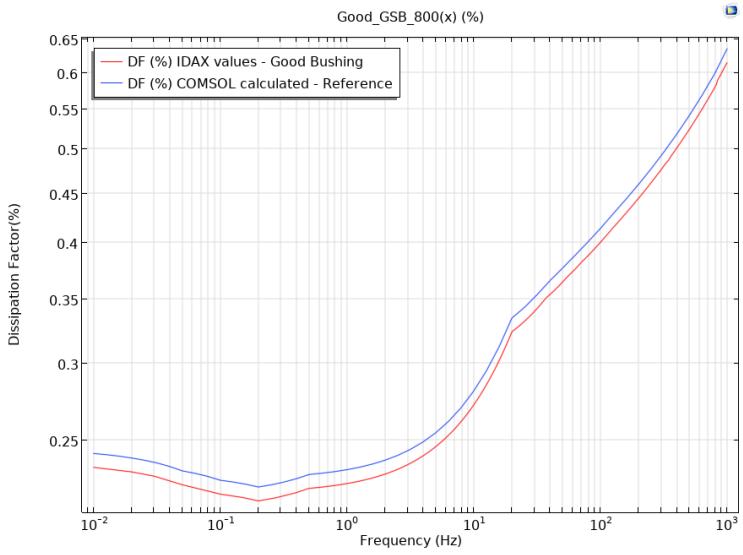

Figure 4.1: COMSOL Model Validation - Electrostatics

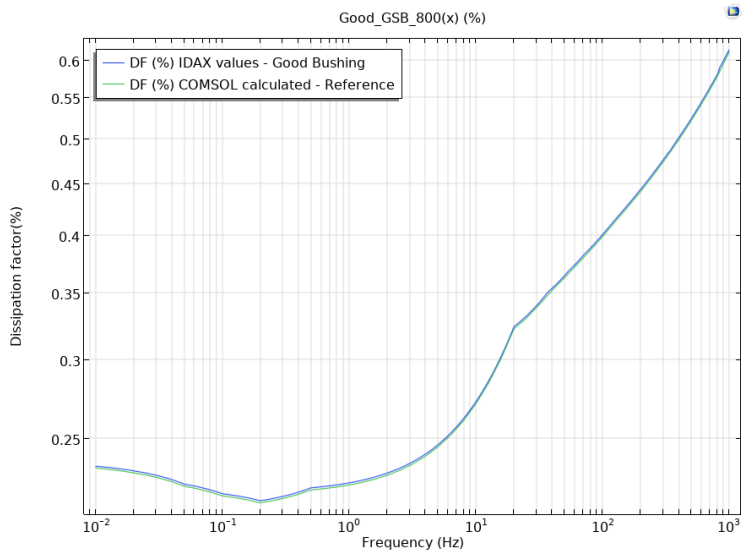

Figure 4.2: COMSOL Model Validation - Electric Currents

In the case of results from electrostatics physics, the table 4.2 show that there is 3.4 % increase in loss factor when compared with IDAX value and the 1.5 % increase in calculated capacitance value. In the case of results from electric current physics, the table 4.3 shows that there is 0.5 % decrease in loss factor when compared with IDAX value and the 5.7 % increase in calculated capacitance value. The difference found between the COMSOL calculated and the experimental values are acceptable since it is very close to the actual values and also within in the acceptable range defined from IEC standard [8].

Values @ 50 Hz	**IDAX Reference**	**COMSOL Calculated**	**% Difference**
tan δ (%)	0.364	0.37622	+3.4%
Capacitance (pF)	690.7	701.6	+1.5%

Table 4.2: Model Validation – Electrostatics

Values @ 50 Hz	**IDAX Reference**	**COMSOL Calculated**	**% Difference**
tan δ (%)	0.364	0.3622	-0.5%
Capacitance (pF)	690.7	730.1	+5.7%

Table 4.3: Model Validation – Electric Currents

4.3 Defects created in the bushing model

In the developed bushing model, the possible defects can be created using the boundary condition under the appropriate physics. This section describes the types of defects applied in the model and the boundary conditions associated with it. The

defect created is further investigated for different conditions to verify the change in loss factor and capacitance values after each computation.

4.3.1 Implementation of Defects - Electrostatics

In electrostatic physics, the stationary study related to electric field is involved and the significant parameter is Relative Permittivity (ε_r) of the material assigned to the respective domain. Under electrostatics, the three boundary conditions used to introduce the defects are *Electric Potential*, *Dielectric Shielding* and *Ground*. The defect *Electric Potential on Outer Sheds* is introduced using *Electric Potential* boundary condition. It requires potential value to be given in the settings window. The other defects *Water at Outer Insulator Layer, Ice & Water layer on the Outer Sheds* are introduced using Dielectric Shielding boundary condition. This condition requires thickness (d_s) and relative permittivity (ε_r) of the material to be inserted to simulate the defect. The defect of grounding the sheds is introduced using *Ground*. The Figures 4.3a and 4.3b show the location of the defect that are introduced in the model.

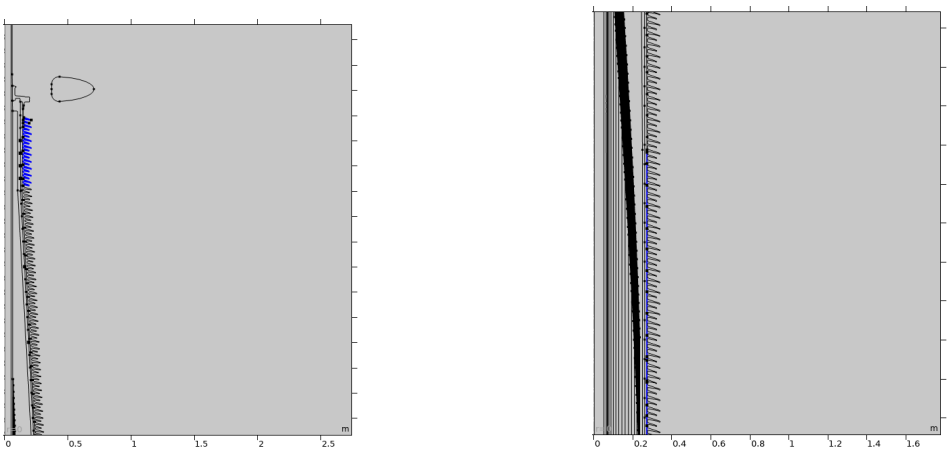

(a) Potential on sheds **(b)** Dielectric Shielding

Figure 4.3: Defect location in the model-Electrostatics

From the Figure 4.4, it is observed that the the loss curve is experienced a shift up or down from the standard reference curve over the chosen frequency range. The defect type, the reference and simulated DF & capacitance value are listed in the table 4.4. For the defect "Electric Potential on Sheds, the loss curve is shifted down with a significant decrease in loss value and increase from capacitance. For the other defects except for the grounded sheds, there is no significant change in the DF value and the capacitance value. In the case of the grounded sheds, the tan δ increased and capacitance decreased from the COMSOL calculated value but the difference from the reference is very minimum as illustrated in the Figure 4.5

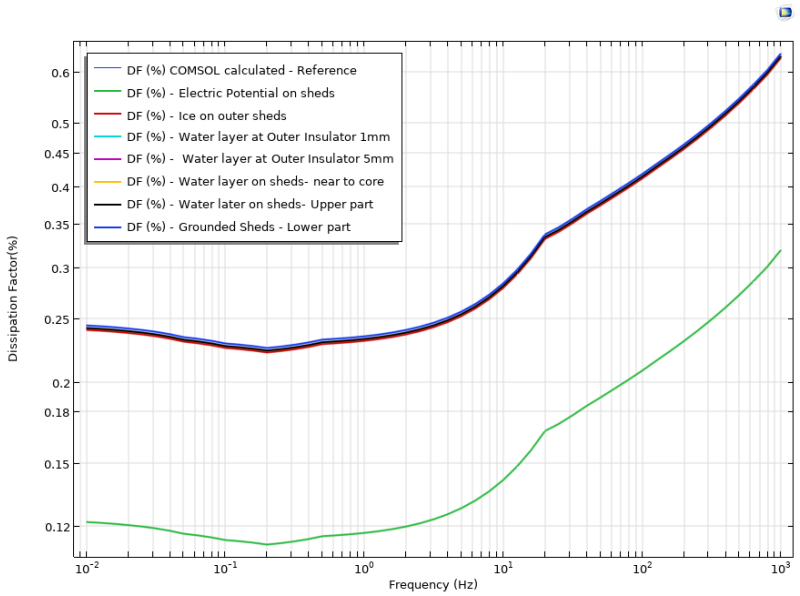

Figure 4.4: Loss curve for defects created - Electrostatics

.

Defect Type	**tan δ (%) @ 50 Hz**	**Capacitance (pF) @ 50 Hz**
Reference (No Defect)	0.3762	701.6
Electric Potential on sheds	0.1892	1436.5
Ice layer in sheds	0.3767	706.5
Water at Outer Insulator layer 1mm	0.3762	701.8
Water at Outer Insulator layer 5mm	0.376	702.1
Water layer at lower part of sheds	0.3761	702.1
Water layer at Upper part of sheds	0.3761	702
Grounded sheds - Lower Part	0.3796	695.2

Table 4.4: Effect of Implemented Defects on tan δ and Capacitance – Electrostatics

It can be inferred that the entire loss curve is shifted up or down depending on the defect type while computing the model for electrostatic physics. Also, the change

observed in DF and capacitance values are not very significant. In this physics, the electric conductivity value does not come into picture and only the relative permittivity value is considered. Electric conductivity of the material aids in better investigation of the DFR pattern for various defects that could occur in the essential parts of the bushing. To include electric conductivity into DFR simulation, the *Electric Current* physics should be assigned for the domain in the developed bushing geometry appropriately as mentioned in the section 3.1.3.2.

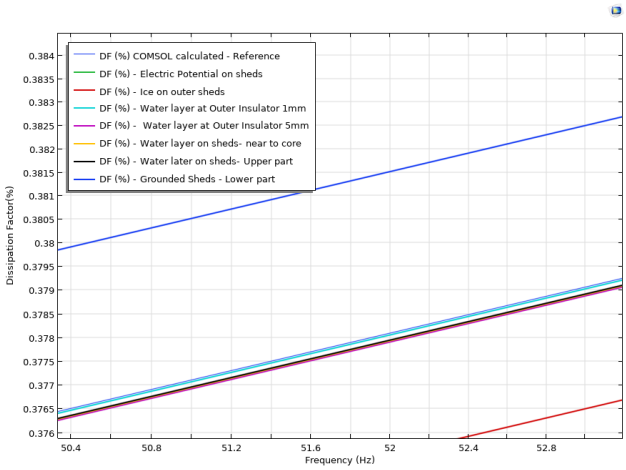

Figure 4.5: Loss curve for defects created - Electrostatics - Zoomed Version

4.3.2 Implementation of Defects - Electric currents

As mentioned in the section 4.3.1, the defects are further created using boundary condition under the physics *Electric Currents* for better analysis of dielectric response of the bushing model for various defects. There are two main boundary conditions - *Electric Potential* and *Electric Shielding* used to introduce the following defects under the electric currents physics. The boundary condition *Electric Potential* is similar to the condition in electrostatic physics and require the boundary selection and the potential value where it is needed to be defined. The *Electric Shielding* boundary condition creates a conductive layer of specified thickness d_s and having the relative permittivity ε_r & conductivity σ in S/m over the selected boundaries in the model.. This formation of conductive layer enables the leakage current to flow in the selected boundary and the current density varies with the thickness d_s and the conductivity σ value.

4.3.2.1 Electric Potential on Sheds

The first defect in electric currents physics to be introduced in the model is creating electric potential on the outer insulator sheds. The electric potential is created on the different part of the sheds to observe the change in loss factor trend, as represented in the Figure 4.6.

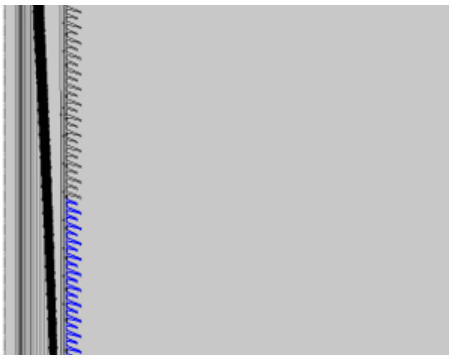

Figure 4.6: Defect Location in the model - Potential on Sheds - Electric Currents

From the Figure 4.7 and the table 4.5, it can be seen that the potential created over the sheds thar are near to the grounded flange shows a visible down shift from the reference curve and a higher increase in the capacitance. While the potential over the sheds in the conical shape transition in the bushing geometry, the curve also shifted down with a increase in capacitance having lesser difference than the former case. There is no impact observed for the potential created near to the sheds of top terminal of the bushing. Therefore, the defect that are in close proximity to the core are captured in the dielectric response and the change varies with how much close the defect lies near to the condenser core where the dielectric losses are being computed.

Defect Type	**tan δ (%) @ 50 Hz**	**Capacitance (pF) @ 50 Hz**
Reference (No Defect)	0.3622	730.1
Sheds - Upper Part	0.3622	730.1
Sheds near conical transition	0.0501	926.7
Sheds - Lower Part	0.0101	12073×10^{-8}

Table 4.5: Electric Potential on Sheds - tan δ and Capacitance

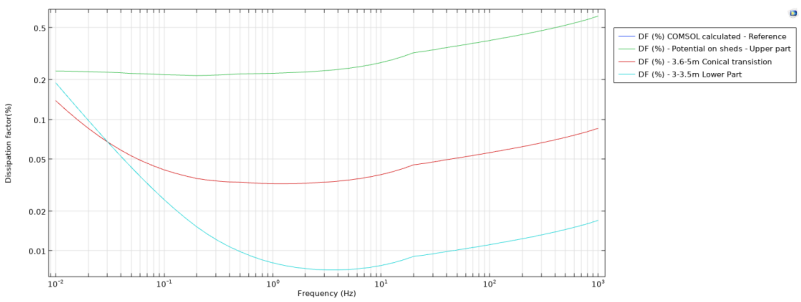

Figure 4.7: Loss curve - Potential on Sheds

4.3.2.2 Pollutant Layer on Sheds

Majority of the transformer bushings are installed at remote places where the external insulator sheds are exposed to various kinds of pollutants from the nearby factories or from the geographical location. Hence, it is decided to study the dielectric response for the effect of pollutant deposition on the sheds. The effect of pollutant can be well investigated when the conductivity of pollutant is included in the study which is well supported by using the electric current physics, as presented in the Figure 4.8. The electric shielding is created on the sheds in the conical part of the bushing since it is found to be a sensitive area.

For the simulation purpose, the electric potential distribution is considered to be uniform across the shielding layer that is formed using the electric shielding boundary condition. But in real time, the pollutant layer on the sheds has non-uniform potential distribution at different points across the layer. Since it is challenging to identify the conductivity value of specific pollutant and hence values are chosen based on conductivity values of pollutants that are found on the outdoor polymeric insulator, given in the study [32]. The layer of pollutant on the shed is realized in the model using electric shielding boundary condition. To study the effect of pollutant deposition in loss factor curve, the thickness of pollutant layer is given as 1 μm, 8 μm, 10 μm and, 100 μm whereas in the real time environment, the layer thickness is in the range of few hundred micrometers depending on the pollution level.

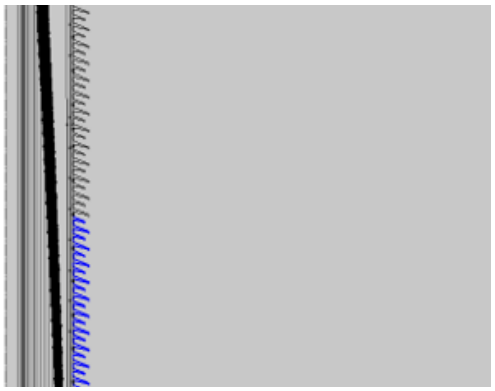

Figure 4.8: Defect Location in the model- Layer of Pollutants with different conductivities

The conductivity values are defined in such a way to analyze the trend of loss factor curve , how it changes with the different values of increased conductivities with increase in layer thickness. From the Figure 4.9, it can be observed that there is an significant increase in loss factor value at the lower frequency range for minimum thickness of 1 μm & 8 μm having conductivity of 1 μS/m. This inference is supported by the fact that the DFR measurements helps in identifying the defects at its early stage by capturing it in the lower frequency range. This helps the customer to further investigate the bushing condition so that the defects can be rectified at an early stage before the effect is realized at the operating frequency 50 Hz.

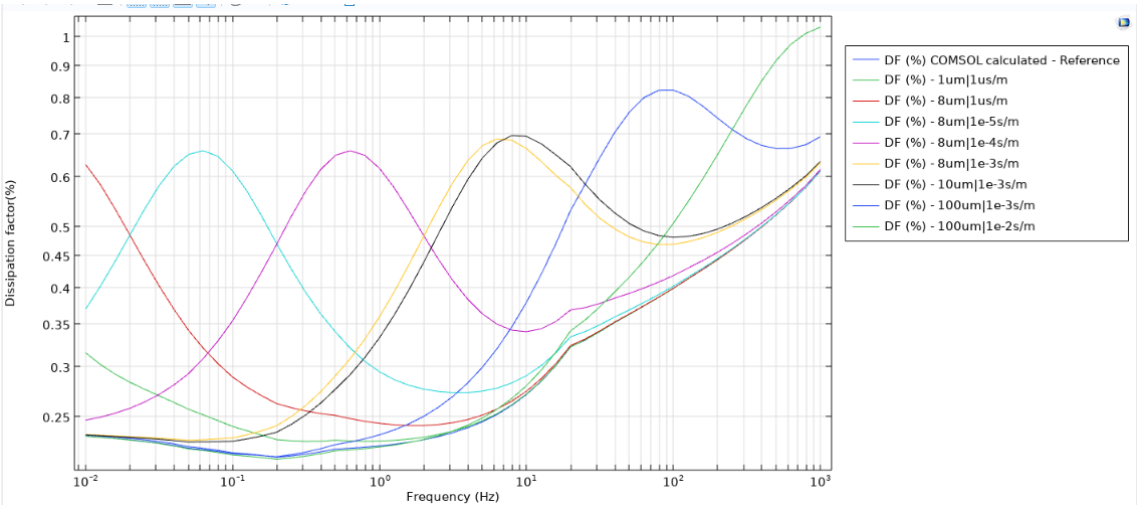

Figure 4.9: Loss curve - Pollutant Layer on Sheds

The noticeable bumps of increased DF value in dielectric response curve is observed at higher frequencies with the increase in conductivity values of pollutants according to the table 4.6. Over the certain of thickness, the peak of loss curve has fallen out of chosen frequency range. Having the same conductivity values and with the increase in layer thickness, the curve pattern hadn't been changed but the loss factor is increased at the specific value of frequency. Besides, there is no significant change in the capacitance value is observed.

Defect Type	**tan δ (%) @ 50 Hz**	**Capacitance (pF) @ 50 Hz**
Reference (No Defect)	0.3622	730.1
$d_s = 1\ \mu m$, $\sigma = 1\ \mu S/m$	0.3623	730.1
$d_s = 8\ \mu m$, $\sigma = 1\ \mu S/m$	0.3629	730.1
$d_s = 8\ \mu m$, $\sigma = 1 \times 10^{-5}$ S/m	0.3682	730.1
$d_s = 8\ \mu m$, $\sigma = 1 \times 10^{-4}$ S/m	0.3911	730.2
$d_s = 8\ \mu m$, $\sigma = 1 \times 10^{-3}$ S/m	0.4804	730.5
$d_s = 10\ \mu m$, $\sigma = 1 \times 10^{-3}$ S/m	0.5047	730.6
$d_s = 100\ \mu m$, $\sigma = 1 \times 10^{-3}$ S/m	0.7576	735
$d_s = 100\ \mu m$, $\sigma = 1 \times 10^{-2}$ S/m	0.4151	736.9

Table 4.6: Pollutant Layer on Sheds - tan δ and Capacitance

4.3.2.3 Water Layer at Outer Insulator

The next defect created in the bushing model is the conductive layer of water at the outer insulator. This defect may occur due to the surface crack in the outer insulator

sheds that induces the moisture ingress in the outer insulator layer. The moisture ingress is recreated in the model using electric shielding boundary condition with the chosen thickness $d_s = 100$ μm and water conductivity $\sigma = 5.5 \times 10^{-6}$ S/m in the settings window. The dielectric response is swept through creating the water later at the different boundaries throughout the length of outer insulator layer as shown in the Figure 4.10.

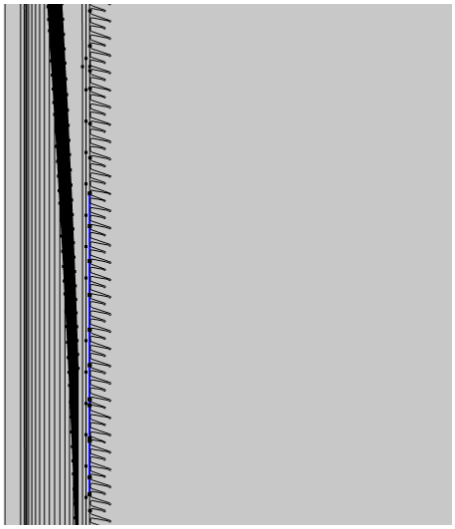

Figure 4.10: Defect Location in the model - Water Layer at Outer Insulator

From the Figure 4.11 and the table 4.7, the visible bumps due to the increased DF value at 1 Hz is observed for the shielding layer which is very near to the core and the next noticeable bump for the increase in the DF value for the shielding layer in the conical transition of the geometry. The DF values at 50 Hz increases as proximity of the conductive layer reduces until certain length of the outer insulator layer. For the water layer near the top terminal, there is no remarkable change in the shape of the response. Besides, there is no change in the capacitance value is observed from its base value.

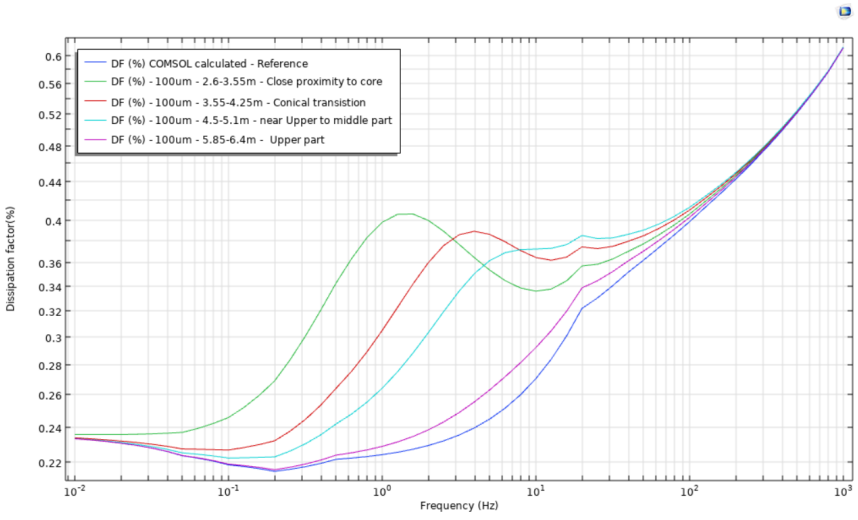

Figure 4.11: Loss curve - Water Layer at Outer Insulator

Defect Location	tan δ (%) @ 50 Hz	Capacitance (pF) @ 50 Hz
Reference (No Defect)	0.3622	730.1
2.6 m-3.55 m - Close proximity to core	0.3771	730.1
3.55 m-4.25 m - Conical transition	0.3847	730.1
4.5 m-5.1 m - near Upper to middle part	0.39	730.1
5.85 m-6.4 m - Upper part	0.3704	730.1

Table 4.7: Water Layer at Outer Insulator - tan δ and Capacitance

4.3.2.4 Water at Gel Layer

The next defect created in the bushing model is the conductive layer of water at the gel layer. This defect may occur due to the improper curing process that leaves the moisture retained within the gel layer. The residual moisture from the curing process is realized in the model using electric shielding boundary condition with the chosen thickness $d_s = 100$ μm & 500 μm, water conductivity $\sigma = 5.5 \times 10^{-6}$ S/m and relative permittivity $\varepsilon_r = 80$ in the settings window. The DFR simulation is swept through creating the water later at the different boundaries throughout the length of gel layer as shown in the Figure 4.12.

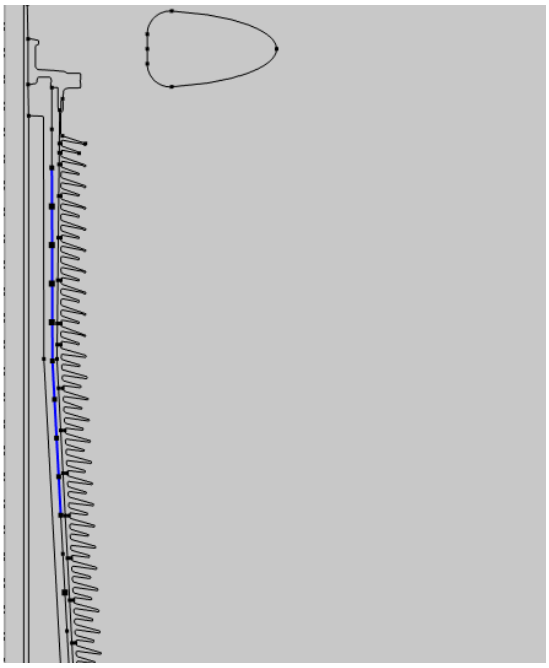

Figure 4.12: Defect Location in the model - Water at Gel Layer

From the Figure 4.13, the similar pattern of loss curve is found as in the case

of water layer at outer insulator. The dielectric response exhibits a remarkable increase which could be noticed from the distinguishable bump (purple in color) for the conductive layer created at the conical transition part of the bushing. Also, for the layer thickness of 100 μm, the DFR captures the defect at its lower frequencies and which are in close proximity to the core. The defect that are away from the condenser core doesn't make any visible change in the response. The corresponding loss factor and capacitance values for d_s 100 μm are listed in the table 4.8. There is no change in the capacitance value is observed from its base value.

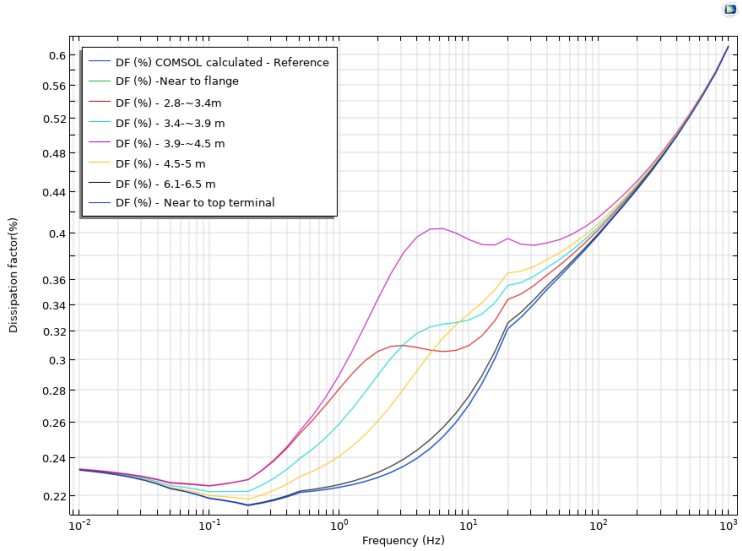

Figure 4.13: Loss curve - Water Layer at Gel Interface - 100 μ m

Defect Location	**tan δ (%) @ 50 Hz**	**Capacitance (pF) @ 50 Hz**
Reference (No Defect)	0.3622	730.1
Near to flange	0.3622	730.1
2.8 m-3.4 m	0.3716	730.1
3.4 m-3.9 m	0.3765	730.1
3.9 m-4.5 m	0.3938	730.1
4.5 m -5 m	0.3822	730.1
6.1-6.5 m	0.3646	730.1
Near to top terminal	0.3622	730.1

Table 4.8: Water at Gel Layer d_s = 100 μm - tan δ and Capacitance

In the case of water layer with thickness 500 μm, the similar pattern of DFR is seen as in the thickness of 100 μm but the bumps in the response is noticed at the

operating frequency, represented in the Figure 4.14. This indicates that the increase in the intensity of the defect is grasped by the DFR at the operating frequency. This in turn triggers the need to further investigation of bushing insulation condition in order to prevent any potential cause of the failure. The corresponding loss factor and capacitance values for d_s 100 μm are listed in the table 4.9.There is no change in the capacitance value is observed from its base value.

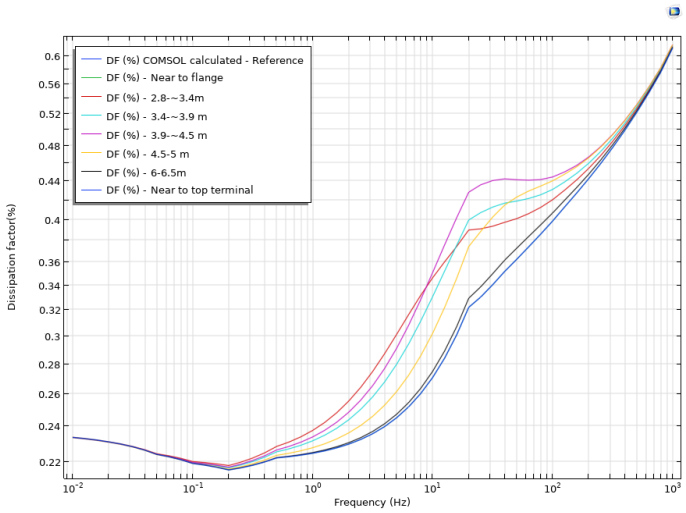

Figure 4.14: Loss curve - Water Layer at Gel Interface - 500 μm

Defect Location	tan δ (%) @ 50 Hz	Capacitance (pF) @ 50 Hz
Reference (No Defect)	0.3622	730.1
Near to flange	0.3622	730.1
2.8 m-3.4 m	0.4005	730.2
3.4 m-3.9 m	0.4183	730.3
3.9 m-4.5 m	0.441	730.4
4.5 m -5 m	0.4225	730.4
6.1-6.5 m	0.3723	730.1
Near to top terminal	0.3622	730.1

Table 4.9: Water at Gel Layer d_s = 500 μm - tan δ and Capacitance

4.3.2.5 Modified Gel Relative Permittivity

The next defect at the material property level studied in the bushing model is the change in the relative permittivity. The gel used here is a mixture and has an ideal value of relative permittivity when it is obtained in proper composition.

Improper composition of gel mixture affects its relative permittivity. There are different composition gel with water and air are applied to analyze whether it is reflected in the DFR response. From the Figure 4.15, it can be noticed that there is no visible change in the response and in the capacitance as well. It aids to conclude that influence of relative permittivity is not pronounced in the DFR simulations. The corresponding loss factor and capacitance values for various gel compositions are listed in the table 4.10.

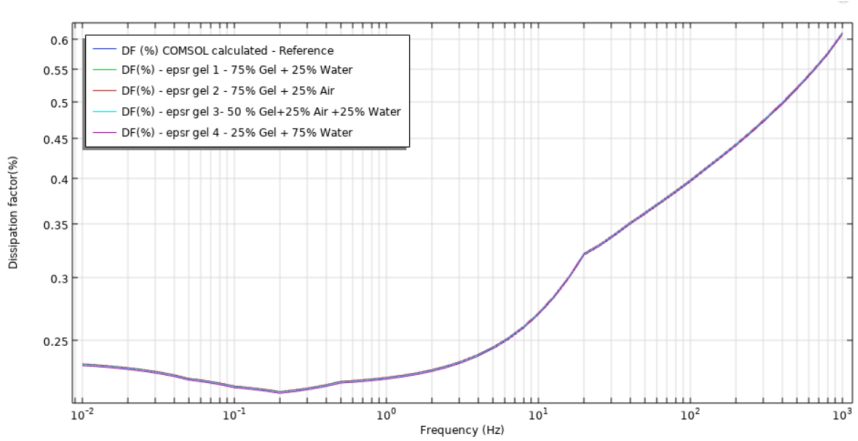

Figure 4.15: Loss curve - Modified Gel Relative Permittivity

Gel composition	**tan δ (%) @ 50 Hz**	**Capacitance (pF) @ 50 Hz**
Reference (No Defect)	0.3622	730.1
75 % Gel + 25 % Water	0.3616	731.3
75 % Gel + 25 % Air	0.3622	730.1
50 % Gel + 25 % Air + 25 % Water	0.3616	731.3
25 % Gel + 75 % Water	0.3601	733.7

Table 4.10: Modified Gel Relative Permittivity - tan δ and Capacitance

4.3.2.6 Layer of Salt Water on Sheds

With the increasing offshore applications, the bushings are increasingly installed in the marine environment. This leads to the higher content of salt deposition on the external insulator sheds. Therefore, it is decided to analyze how the salt layer on the sheds impact in the dielectric response. The salt layer deposition recreated as a layer of salt water in the bushing model by using electric shielding boundary condition with the chosen range of thickness d_s and salt conductivity $\sigma = 4.1$ S/m in the settings window.The electric shielding is created on the sheds in the conical part of the bushing as shown in the Figure 4.16. The salt conductivity varies depending

on the salinity level and the chosen conductivity value of 4.1 S/m that corresponds to 28 kg/m^3 [33].

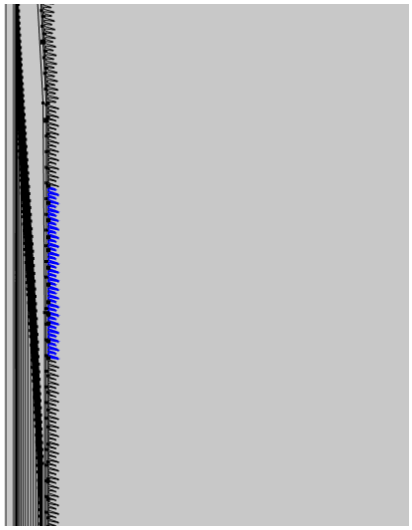

Figure 4.16: Defect Location in the model — Salt water on sheds

From the loss factor curve presented in the Figure 4.17, the important observation can be seen as the loss factor greatly varies only in the lower frequency range irrespective of the increase in thickness. The DF values do not vary significantly at the operating frequency range.The loss factor and capacitance values for various d_s values of salt water are listed in the table 4.11.There is no significant change in the capacitance value is observed from its base value.

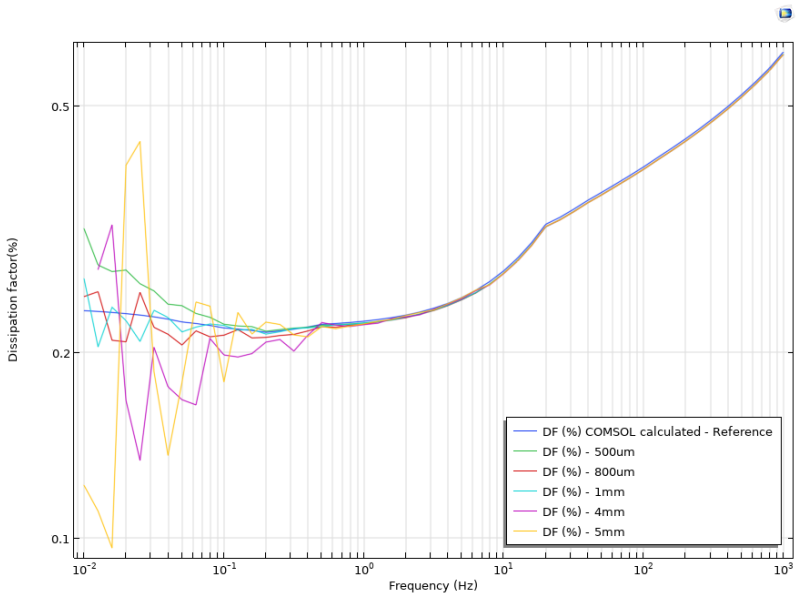

Figure 4.17: Loss curve - Salt water on sheds

Defect level	tan δ (%) @ 50 Hz	Capacitance (pF) @ 50 Hz
Reference (No Defect)	0.3622	730.1
d $_s$ = 500 μm	0.359	736.8
d $_s$ = 800 μm	0.3589	736.8
d $_s$ = 1 mm	0.3589	736.8
d $_s$ = 4 mm	0.3587	736.8
d $_s$ = 5 mm	0.3588	736.8

Table 4.11: Layer of Salt Water on Sheds - tan δ and Capacitance

4.3.2.7 Layer of Snow Deposition on Sheds

In the case of bushing installed in the colder regions, the snow deposition on the external sheds becomes unavoidable. Therefore, to investigate its effect on DFR, the snow layer is created on the outer sheds using the electric shielding boundary condition in the bushing model. The boundaries are defined in such a way that it replicates the deposition of snow on the sheds randomly along its length as shown in the Figure 4.18. The required parameters that need to be specified are relative permittivity ε_r, conductivity σ and the layer thickness d_s of the snow deposited. The relative permittivity of 15 and conductivity of 1×10^{-7} S/m are defined that corresponds to granular snow (dry snow) at -10°C [34]. The range of snow thickness is chosen from 1 cm to 5 cm and it is specified as the d_s value.

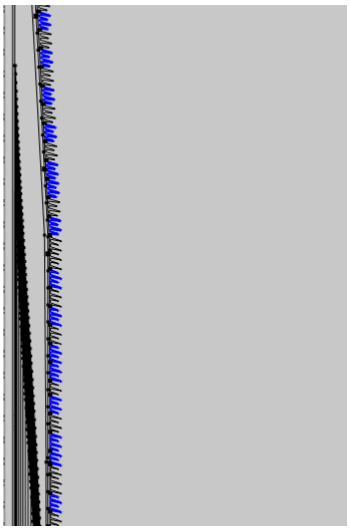

Figure 4.18: Defect Location in the model - Snow Deposition on Sheds

From the Figure 4.19, the response can be seen with a substantial shift from its reference curve. The shift was not prominent at the higher and lower frequency region. It is important to note that the dielectric response curve for d_s = 1 cm

shifted upwards and then the curve shifted down in the similar fashion with the increase in thickness. This is due to the fact that the increase in thickness of snow acts as shielding to the insulator sheds. The denser snow becomes highly resistive and behaves as dielectric shielding to the sheds.The loss factor and capacitance values for various d_s values of snow thickness are listed in the table 4.12.

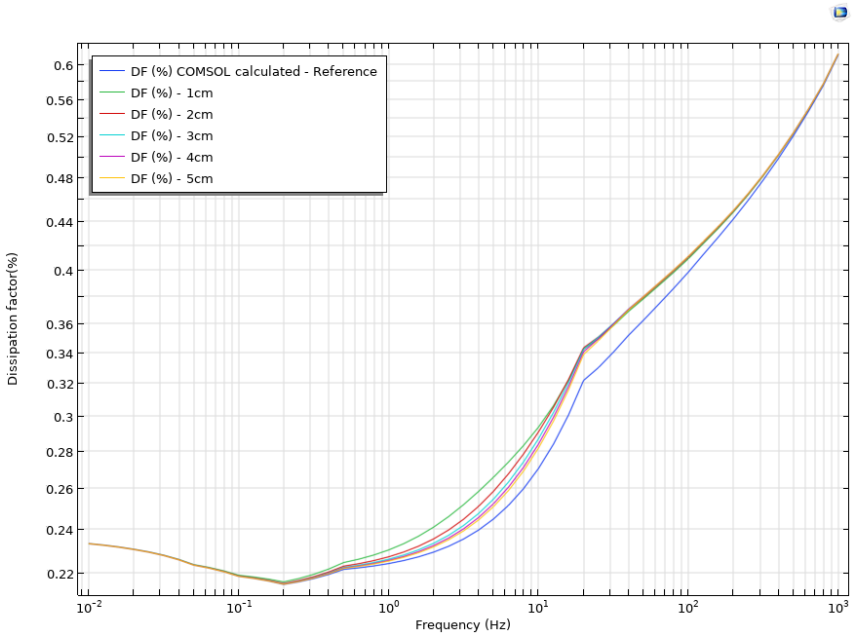

Figure 4.19: Loss curve - Snow Deposition on Sheds

Defect level	**tan δ (%) @ 50 Hz**	**Capacitance (pF) @ 50 Hz**
Reference (No Defect)	0.3622	730.1
d_s = 1 cm	0.3778	730.3
d_s = 2 cm	0.3788	730.4
d_s = 3 cm	0.3794	730.4
d_s = 4 cm	0.3795	730.4
d_s = 5 cm	0.3794	730.5

Table 4.12: Layer of Snow Deposition on Sheds - tan δ and Capacitance

4.3.2.8 Sheds Covered with Snow

Like in the previous section, the identical parameters are given but the difference lies in the selection of boundaries where the shielding condition applies. The boundary condition is created on the sheds partly in the conical part of the bushing as shown in the Figure 4.20.

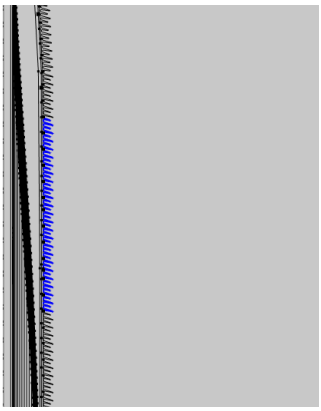

Figure 4.20: Defect Location in the model-Sheds Covered with Snow

The similar response is observed in the previous case but with the significant increase in DF values with visible bumps in the response, as illustrated in the Figure 4.21. This is due to the increase in flow of leakage current due to the formation of conductive path when compared to the previous case. The loss factor and capacitance values for various d_s values of snow thickness on continuous sheds are listed in the table 4.13.

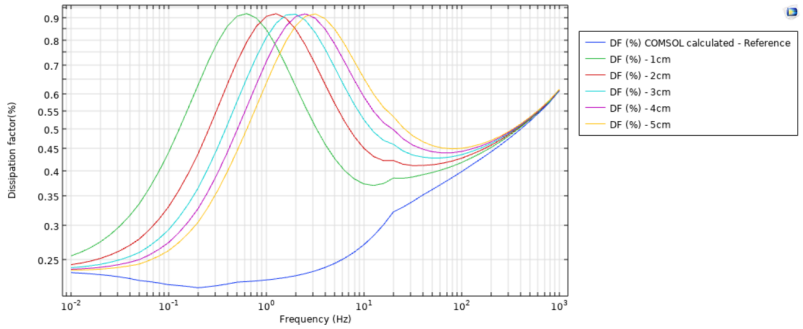

Figure 4.21: Loss curve - Sheds Covered with Snow

Defect level	**tan δ (%) @ 50 Hz**	**Capacitance (pF) @ 50 Hz**
Reference (No Defect)	0.3622	730.1
d_s = 1 cm	0.3963	730.3
d_s = 2 cm	0.4128	730.5
d_s = 3 cm	0.4273	730.6
d_s = 4 cm	0.4423	730.7
d_s = 5 cm	0.4569	730.7

Table 4.13: Sheds Covered with Snow - tan δ and Capacitance

4.3.2.9 Water bubbles at the gel interface

The previous defects are all based on defining the boundary condition and specifying the required parameters. The defect and the resultant DFR discussed in this section are created at the geometry level. In real time, a water bubble may retain at the interface between the gel and the outer insulator layer. An array of 2x30 circles is formed as shown in the Figure 4.22, realised as bubbles filled with water. The appropriate physics is assigned to the array of bubbles to include in the DFR simulations.

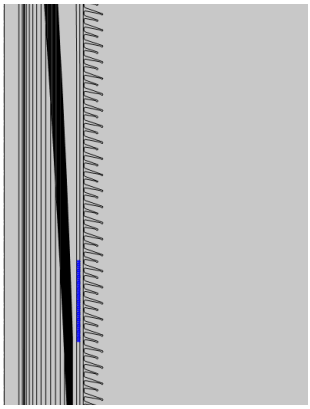

Figure 4.22: Defect Location in the model-Water bubbles at the gel interface

The loss curve and capacitance do not vary over the entire range of frequencies according to the Figure 4.23. The array of water bubbles is placed at different positions at the gel interface, but there is no change in the response observed. The computed loss factor and capacitance values of water bubbles placed at different positions at the gel interface are given in the table 4.14. It can be inferred that DFR fails to capture the presence of water bubbles at the lowest measurement voltage of 140V.

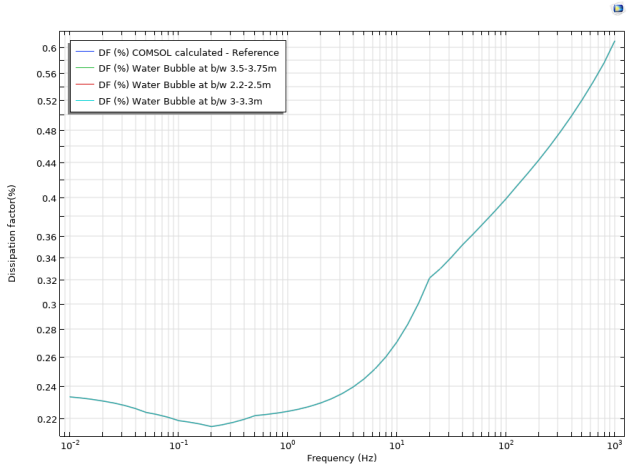

Figure 4.23: Loss curve - Water bubbles at the gel interface

Defect Location	tan δ (%) @ 50 Hz	Capacitance (pF) @ 50 Hz
Reference (No Defect)	0.3622	730.1
Between 3.5 m - 3.75 m	0.3622	730.1
Between 2.2 m - 2.5 m	0.3622	730.1
Between 3 m - 3.3 m	0.3622	730.1

Table 4.14: Water bubbles at the gel interface - tan δ and Capacitance

4.3.2.10 Grounding of few outermost foils

The next defect studied arises from unintentional grounding of outermost foils in the condenser core. The defect is introduced in the core by assigning the ground to few outermost foils as illustrated in the Figure 4.24.From the figure 4.25, it is observed that the loss factor do not vary significantly. On the other hand, the capacitance increases to the considerable extent as showcased in the table 4.15. The capacitance graded bushing consists of capacitors evenly distributed in series manner. Hence, grounding few outermost foils results in increase in the equivalent capacitance.

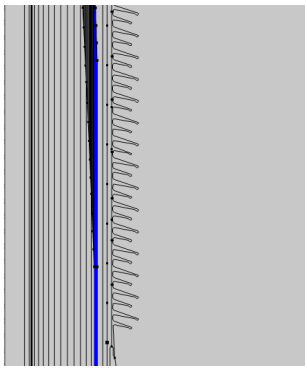

Figure 4.24: Defect Location in the model-Grounding of few outermost foils

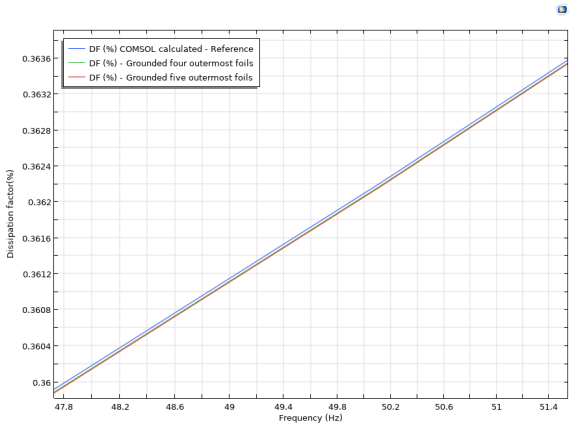

Figure 4.25: Loss curve - Grounding of few outermost foils

Defect level	tan δ (%) @ 50 Hz	Capacitance (pF) @ 50 Hz
Reference (No Defect)	0.3622	730.1
Grounded four outermost foils	0.3621	755.6
Grounded five outermost foils	0.3621	764.8

Table 4.15: Grounding of few outermost foils - tan δ and Capacitance

4.3.2.11 Short circuiting of foils

The final defect studied is caused from short circuit between the conductive layers i.e., foils in the condenser core. The defect is introduced in the core by assigning the same floating potential to full foils in the middle part of the core and to the foils near to the flange, as illustrated in the Figure 4.26.

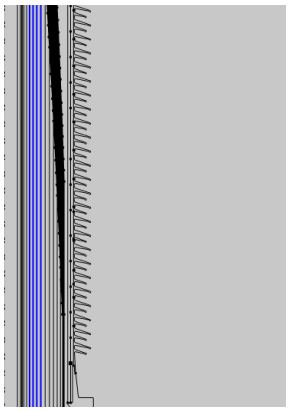

Figure 4.26: Defect Location in the model-Short circuiting of foils

From the figure 4.27, it is observed that the loss factor do not vary significantly. On the other hand, the capacitance greatly increases as shown in the table 4.16. By short circuiting the foils, the equivalent capacitance of the core is greatly increased.

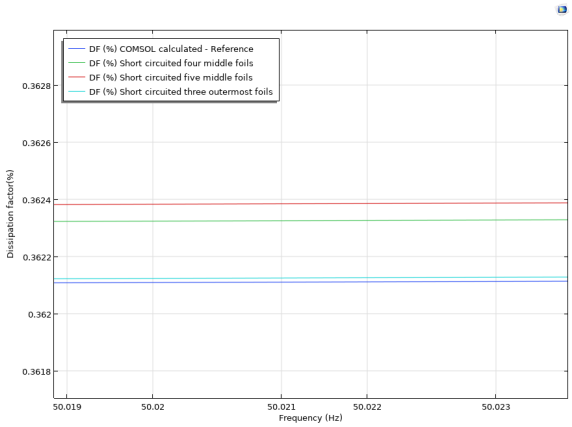

Figure 4.27: Loss curve - Short circuiting of foils

Defect level	**tan δ (%) @ 50 Hz**	**Capacitance (pF) @ 50 Hz**
Reference (No Defect)	0.3622	730.1
Short circuited four middle foils	0.3624	987.2
Short circuited five middle foils	0.3624	1122.2
Short circuited three outermost foils	0.3622	870.3

Table 4.16: Short circuiting of foils - tan δ and Capacitance

5
Conclusion

5.1 Discussion

The results obtained from DFR simulations for various defects seem to be reliable and it can provide a base line of prediction to identify the defects within the bushing insulation. It can be concluded from the loss factor plots that the defect can be identified early by measuring dielectric response over the wide range of frequencies. The defect is well captured by the DFR when the location of defect lies in close proximity to the condenser core. If the defect lies far away from the core, the trend of tan δ curve does not bring significant change from the reference curve. The amount of change indicates that how close the defect lies to the condenser core and how intense the defect is in the core or other parts of the bushing. In the case of bushing model assigned with electrostatic physics, the dielectric response shifts up or down and there were no any noticeable bumps in the response. While in the case of model assigned with electric current physics, the bumps are prominent in the tan δ curve for the implemented defects. The bumps in the loss factor curve tend to appear in the certain frequency range depending on the intensity of the defect. If the intensity of the defect is less, it appears in the lower frequency region which aids in the identification of defects at an early stage.If the intensity of the defect is high, then bumps appear in the operating frequency which triggers the immediate investigation of bushing condition to prevent its failure. For the defects created within in the condenser core, the prominent change in capacitance was observed while the DF value do not vary over the entire frequency range. The defects that are created over the conical transition in the bushing geometry are captured by the DFR simulations. On the whole, the DFR simulations help to predict the type of the defect but the real challenge with DFR is to identify the root cause and location of the defect.

5.2 Future Work

From the thesis work, it is clear that DFR provides a base line to predict the defect type. Hence, more combination of defects that occur in real time bushing operation could be implemented using the suitable boundary condition under the appropriate physics to study the impact on the loss factor curve. Secondly, more number of real time DFR experimental data would be required to improve the accuracy of the COMSOL model so that it provides results with higher degree of reliability. The study of PD by DFR simulation will be new area to investigate in the future.

Bibliography

[1] Egypt Business Directory. *Global Large Power Transformers Sales Market and Forecast Report 2016–2021.* Available online: https://www.egypt-business.com/ticker/details/1645-global-large-power-transformers-sales-market-and-forecast-\report-2016-2021/66091 (Accessed: May 20, 2025)

[2] V. Lebedev, "Transformer basics," in *2007 Electrical Insulation Conference and Electrical Manufacturing Expo*, 2007, pp. 356–359. doi: 10.1109/EEIC.2007.4562642.

[3] Hillary, W.D.A.G. & Jayarathna, K.L.I.M & Ranasinghe, Lahiruni & Samarakoon, Bhagya & Rathnayake, N.M.T.N. & Lucas, Rohan & Samarasinghe, Rasara. (2017). A tool for estimating remaining life time of a power transformer. 373-378. 10.1109/MERCon.2017.7980513.

[4] A. Küchler, *High Voltage Engineering: Fundamentals, Technology, Applications*. Germany: Springer Verlag, 2018. ISBN: 978-3-642-11992-7.

[5] Hugh M. Ryan, *High Voltage Engineering and Testing, 2nd Edition*. London: The Institution of Electrical Engineers, 2001.

[6] James H. Harlow, *Electric Power Transfomer Engineering*. USA: The Electric Power Engineering Series ; 9, ISBN 0-8493-1704-5.

[7] IEEE Standard for General Requirements and Test Procedure for Power Apparatus Bushings," in IEEE Std C57.19.00-2023 (Revision of IEEE Std C57.19.00-2004) , vol., no., pp.1-32, 15 May 2023, doi: 10.1109/IEEESTD.2023.10123335.

[8] International Electrotechnical Commission,"IEC 60137: Insulated bushings for alternating voltages above 1000 V," IEC Standard, 11th ed., 2017.

[9] IEEE Guide for the Dielectric Frequency Response Measurement of Bushings," in IEEE Std C57.12.200-2022 , vol., no., pp.1-84, 27 Jan. 2023, doi: 10.1109/IEEESTD.2022.10026269.

[10] Zeeshan Ahmed, *Analysis of Partial Discharge in OIP Bushing Models*, Degree Project in Electromagnetic Engineering, School of Electrical Engineering, Kungliga Tekniska Högskolan,Stockholm, 2011.

[11] G. B. Gharehpetian, H. Karami, and S.-A. Ahmadi, "Chapter 1 - An introduction to power transformer monitoring," in *Power Transformer Online Monitoring Using Electromagnetic Waves*, G. B. Gharehpetian and H. Karami, Eds. Academic Press, 2023, pp. 1–12. ISBN: 978-0-12-822801-2. doi: 10.1016/B978-0-12-822801-2.00001-X.

[12] "Power Transformer Complete Accessories," *Electrical-Tech*. [Online]. Available: https://electricaltech.in/power-transformer-complete-accessories/. [Accessed: Apr. 20, 2025].

[13] F. Vahidi and S. Tenbohlen, "Statistical Failure Analysis of European Substation Transformers," in *Diagnostik elektrischer Betriebsmittel 2014 – Beiträge der 6. ETG-Fachtagung*, Berlin, Germany, Nov. 2014. Available: https://www.researchgate.net/publication/272088767_Statistical_Failure_Analysis_of_European_Substation_Transformers

[14] S. Tenbohlen, Z. Hanif, and D. Martin, "Analysis of Major Failures of Power Transformers," presented at the ICTRAM Conference, Split, Croatia, Nov. 2023. Available: https://www.researchgate.net/publication/375860407_Analysis_of_Major_Failures_of_Power_Transformers

[15] M. Tozzi, "Bushing Failure Prevention Through Online Monitoring," *Power Systems Technology*, [Online]. Available: https://www.powersystems.technology/community-hub/technical-articles/bushing-failure-prevention-through-online-monitoring. [Accessed: Apr. 20, 2025].

[16] "Why high voltage power equipments need to install Corona rings" *Artisan Industry* . [Online]. Available: https://www.coronarings.com/blog/why-high-voltage-power-equipments-need-to-install-corona-rings-\corona/. [Accessed: May. 04, 2025].

[17] INMR- Enriching Technical Knowledge of T&D Professionals, *Introduction-Transformer Bushings*, Synthetic Dry Type Bushings Applied to HV Transformers & Reactors (Video), 2022. Available at: https://www.inmr.com/synthetic-dry-type-bushings-applied-power-transformers-video/ [Accessed: April 22, 2025].

[18] "Bushings," *Reinhausen*. [Online]. Available: https://www.reinhausen.com/portfolio/bushings. [Accessed: Apr. 27, 2025].

[19] "Wall Bushings," *Team Chain*. [Online]. Available: http://en.teamchain.com/product/69.html. [Accessed: Apr. 27, 2025].

[20] *Engineering Resource*. [Online]. Available: https://engrr.com/. [Accessed: Apr. 29, 2025].

[21] "Diagnostic testing of bushings," *Megger*. [Online]. Available: https://www.megger.com/en-gb/et-online/august-2021/diagnostic-testing-of-bushings. [Accessed: May 06, 2025].

[22] M. Tozzi, "Three Steps for Diagnostic Testing of Bushings," *Power Systems Technology*, [Online]. Available: https://www.powersystems.technology/community-hub/technical-articles/three-steps-for-diagnostic-testing-of-bushings-transformer-\technology-digital-community-article.html. [Accessed: August. 06, 2025].

[23] Power Systems Technology, "Transformer Bushings: How to Detect Incipient Faults in an Early Stage," *Power Systems Technology*, [Online]. Available: https://www.powersystems.technology/community-hub/technical-articles/transformer-bushings-how-to-detect-incipient-faults-in-an-early-\stage. [Accessed: 8-May-2025].

[24] D. Broek, "The Finite Element Method: Introduction," *Academia.edu*, [Online]. Available: https://www.academia.edu/5199290/THE_FINITE_

ELEMENT_METHOD_INTRODUCTION. [Accessed: 8-May-2025].

[25] COMSOL AB, "COMSOL Multiphysics® v. 6.3," https://www.comsol.com, Stockholm, Sweden, 2024.[Accessed: 09-May-2025]

[26] COMSOL AB, "AC/DC Module User's Guide," http://localhost:8090/docserver/#!/com.comsol.help.acdc/acdc_ug_electric_fields.07.002.html?type=ext, COMSOL Multiphysics® v. 6.3, Stockholm, Sweden, 2024. Accessed: May 10, 2025.

[27] COMSOL AB, "AC/DC Module User's Guide," http://localhost:8090/docserver/#!/com.comsol.help.acdc/acdc_ug_electric_fields.07.048.html?type=ext, COMSOL Multiphysics® v. 6.3, Stockholm, Sweden, 2024. Accessed: May 10, 2025

[28] Wuhan Goldsol Co. Ltd., "FDS-PDC Dielectric Frequency Response Analyzer (DRA-3000)," [Online]. Available: https://www.vlf-test.com/html_products/FDS-PDC-dielectric-frequency-response-analyzer-182.html. [Accessed: May 12, 2025].

[29] OMICRON electronics, "DIRANA – Dielectric Frequency Response Analyzer," [Online]. Available: https://www.omicronenergy.com/en/products/dirana/. [Accessed: May 12, 2025].

[30] Megger, "IDAX series of insulation diagnostic analyzers," [online]. Available: https://www.megger.com/sv/PRODUKTER/idax-serien-med-analysatorer-isoleringsdiagnostik#information. [Accessed: May 12, 2025]

[31] D. J. Smith, S. G. McMeekin, B. G. Stewart, and P. A. Wallace, *Modelling the Effects of Temperature and Moisture Ingress on Capacitance and Dissipation Factor Measurements within Oil Impregnated Paper Transformer Bushings*, Proceedings of the COMSOL Conference 2010, Paris, 2010.

[32] Arshad, M., Nekahi, A., McMeekin, S.G., and Farzaneh, M., *Effect of Pollution Layer Conductivity and Thickness on Electric Field Distribution along a Polymeric Insulator*, School of Engineering and Built Environment, Glasgow Caledonian University, and Canada Research Chair on Atmospheric Icing Engineering of Power Networks (INGIVRE), Université du Québec à Chicoutimi, QC, Canada.

[33] Bureau of Indian Standards, *Artificial Pollution Test on High Voltage Insulators to be Used on AC Systems (First Revision)*

[34] S. Evans, *Dielectric Properties of Ice and Snow—A Review*, Scott Polar Research Institute, Cambridge, England.

A

Appendix

The method or code for creation of foils, deletion of foils, assigning and removing floating potential to the foils are given here. The code originally written by Maria Arvidsson, employee at Hitachi Energy Sweden AB and the code has been enhanced to attain the intended outcome.

A.1 Creation of Foils in Bushing Geometry

```
// Reading Foildata
String[][] foil_parameters = readExcelFile("
   GSB800_ext06_olin_FOD_FOD6210_10% _20230109_enligt
   lindningsritning.xlsm", "ANALYSIS", "D16"); // diameter
   and length of create_foils
String[][] foil_type = readExcelFile("
   GSB800_ext06_olin_FOD_FOD6210_10% _20230109_enligt
   lindningsritning.xlsm", "ANALYSIS", "C16"); // full or
   partial foil
String[][] Outer_Diameter = readExcelFile("
   GSB800_ext06_olin_FOD_FOD6210_10% _20230109_enligt
   lindningsritning.xlsm", "DESIGN", "F13"); // read outer
   diameter as string from DESIGN sheet

//double cond_OD = 0.125;


int rows = foil_parameters.length; //Number of rows in excel
   sheet "ANALYSIS", equals number of create_foils
int columns = 5;
double[][] create_foils = new double[rows][columns];

// Turning string matrix into matrix with numbers using for
   loops. For tube/foil
for (int i = 0; i < rows; i++) { //looping over every row
  for (int j = 0; j < columns; j++) {
    double value = Double.parseDouble(foil_parameters[i][j]);
        //Changing type from String to Double.
    double scale = 0.001; //Excel sheet value is in [mm].
       Scaling to [m] for COMSOL
    create_foils[i][j] = value*scale; //Changing [mm] to [m]
```

```
  }
}

// Data for if the foil is partial or full (PorF)
int row = foil_type.length;
//int full_foil = -1; //full foil
//int partial_foil = 0; // partial foil
model.component("comp1").geom("geom1").nodeGroup().create("
    grp1");
model.component("comp1").geom("geom1").nodeGroup("grp1").
    label("Full_foils");

model.component("comp1").geom("geom1").nodeGroup().create("
    grp2");
model.component("comp1").geom("geom1").nodeGroup("grp2").
    label("PFU_foils");

model.component("comp1").geom("geom1").nodeGroup().create("
    grp3");
model.component("comp1").geom("geom1").nodeGroup("grp3").
    label("PFL_foils");

for (int k = 0; k < row; k++) {
  if (create_foils[k][2] == create_foils[k][3]) { // Create
      full create_foils, if the cells are the same then it is
      a full foil
    String foilTag = "bF"+k+" full"; //Name of foil

    model.component("comp1").geom("geom1").create(foilTag, "
        BezierPolygon"); //Creating geometry object
    model.component("comp1").geom("geom1").feature(foilTag).
        set("type", "solid"); //Setting geometry object
        features
    model.component("comp1").geom("geom1").feature(foilTag).
        set("p", new double[][]{{create_foils[k][0]/2,
        create_foils[k][0]/2}, {create_foils[k][1],
        create_foils[k][4]}}); //foil placement
    model.component("comp1").geom("geom1").feature(foilTag).
        set("degree", 1); //1D object
    model.component("comp1").geom("geom1").run(foilTag); //
        Building foil
    model.component("comp1").geom("geom1").nodeGroup("grp1").
        add(foilTag);


    // Adding a cumulative selection for each full foil
    String nameFF = "FF"+k; // This is the label for the
        cumulative selection, FF = Full Foil
```

```
    String selFF = "selFF"+k; // This is the "name" of the
        cumulative selection
    model.component("comp1").geom("geom1").feature(foilTag).
        set("w", new int[]{1, 1});
    model.component("comp1").geom("geom1").selection().create
        (selFF, "CumulativeSelection");
    model.component("comp1").geom("geom1").selection(selFF).
        label(nameFF);
    model.component("comp1").geom("geom1").feature(foilTag).
        set("contributeto", selFF);
} else { //Creating upper partial foil
    String foilTag1 = "b"+k+" partial upp"; //Name of upper
        partial foil
    model.component("comp1").geom("geom1").create(foilTag1, "
        BezierPolygon"); //Creating geometry object
    model.component("comp1").geom("geom1").feature(foilTag1).
        set("type", "solid"); //Setting geometry object
        features
    model.component("comp1").geom("geom1").feature(foilTag1).
        set("p", new double[][]{{create_foils[k][0]/2,
        create_foils[k][0]/2}, {create_foils[k][1],
        create_foils[k][2]}}); //foil placement
    model.component("comp1").geom("geom1").feature(foilTag1).
        set("degree", 1); //1D object
    model.component("comp1").geom("geom1").run(foilTag1); //
        Building foil
    model.component("comp1").geom("geom1").nodeGroup("grp2").
        add(foilTag1);

    // Adding a cumulative selection for each upper partial
        foil
    String namePFU = "PFU"+k; // PFU = Partial Foil Upper
    String selPFU = "selPFU"+k;
    model.component("comp1").geom("geom1").feature(foilTag1).
        set("w", new int[]{1, 1});
    model.component("comp1").geom("geom1").selection().create
        (selPFU, "CumulativeSelection");
    model.component("comp1").geom("geom1").selection(selPFU).
        label(namePFU);
    model.component("comp1").geom("geom1").feature(foilTag1).
        set("contributeto", selPFU);

    // Creating lower partial foil
    String foilTag2 = "b"+k+" partial low"; //Name of lower
        partial foil
    model.component("comp1").geom("geom1").create(foilTag2, "
        BezierPolygon"); //Creating geometry object
    model.component("comp1").geom("geom1").feature(foilTag2).
        set("type", "solid"); //Setting geometry object
```

```
        features
    model.component("comp1").geom("geom1").feature(foilTag2).
        set("p", new double[][]{{create_foils[k][0]/2,
        create_foils[k][0]/2}, {create_foils[k][3],
        create_foils[k][4]}}); //foil placement
    model.component("comp1").geom("geom1").feature(foilTag2).
        set("degree", 1); // 1D object
    model.component("comp1").geom("geom1").run(foilTag2); //
        Building foil
    model.component("comp1").geom("geom1").nodeGroup("grp3").
        add(foilTag2);

    // Adding a cumulative selection for each lower partial
        foil
    String namePFL = "PFL"+k; // PFL = Partial Foil Lower
    String selPFL = "selPFL"+k;
    model.component("comp1").geom("geom1").feature(foilTag2).
        set("w", new int[]{1, 1});
    model.component("comp1").geom("geom1").selection().create
        (selPFL, "CumulativeSelection");
    model.component("comp1").geom("geom1").selection(selPFL).
        label(namePFL);
    model.component("comp1").geom("geom1").feature(foilTag2).
        set("contributeto", selPFL);
  }
}
//---------------------------------------------------------
// Enclose the create_foils in order to have a closed
    geometry
// Connect the end points of the create_foils and connect
    with a line to the conductor.

// 1. Draw lines between upper create_foils
for (int m = 0; m < rows-1; m++) {
  String UpperLine = "L"+m+" upper line"; //Name of upper
      partial foil
  model.component("comp1").geom("geom1").create(UpperLine, "
      LineSegment"); //Creating geometry object
  model.component("comp1").geom("geom1").feature(UpperLine).
      set("specify1", "coord"); //Setting geometry object
      features
  model.component("comp1").geom("geom1").feature(UpperLine).
      set("specify2", "coord");
  model.component("comp1").geom("geom1").feature(UpperLine).
      set("coord1", new double[]{create_foils[m][0]/2,
      create_foils[m][1]}); // Start point
  model.component("comp1").geom("geom1").feature(UpperLine).
      set("coord2", new double[]{create_foils[m+1][0]/2,
      create_foils[m+1][1]}); // End point
```

```
  model.component("comp1").geom("geom1").run(UpperLine); //
     Creating line
}

// 2. Draw lines between lower create_foils
for (int m = 0; m < rows-1; m++) {
  String LowerLine = "L"+m+" lower line"; //Name of upper
     foil
  model.component("comp1").geom("geom1").create(LowerLine, "
     LineSegment"); //Creating geometry object
  model.component("comp1").geom("geom1").feature(LowerLine).
     set("specify1", "coord"); //Setting geometry object
     features
  model.component("comp1").geom("geom1").feature(LowerLine).
     set("specify2", "coord");
  model.component("comp1").geom("geom1").feature(LowerLine).
     set("coord1", new double[]{create_foils[m][0]/2,
     create_foils[m][4]}); // Start point
  model.component("comp1").geom("geom1").feature(LowerLine).
     set("coord2", new double[]{create_foils[m+1][0]/2,
     create_foils[m+1][4]}); // End point
  model.component("comp1").geom("geom1").run(LowerLine); //
     Creating line
}

//-------------------------------------------------------------
// 3. Draw lines between the conductor and the create_foils

// For outer diameter (OD)
int rowsOD = 1;
int columnsOD = Outer_Diameter[0].length;
double[][] OD = new double[rowsOD][columnsOD];

for (int c = 0; c < rowsOD; c++) {
  for (int d = 0; d < columnsOD; d++) {
    if (Outer_Diameter[c][d] == "String[][]") {
      Outer_Diameter[c][d] = "0";
    } else {
      double valueOD = Double.parseDouble(Outer_Diameter[c][d
         ]);
      double scaleOD = 0.001;
      OD[c][d] = valueOD*scaleOD; // converting [mm] to [m]
    }
  }
}

// creating lines for partial foils

String Line = "L"; //Name of upper partial foil
```

```
model.component("comp1").geom("geom1").create(Line, "
    LineSegment"); //Creating geometry object
model.component("comp1").geom("geom1").feature(Line).set("
    specify1", "coord"); //Setting geometry object features
model.component("comp1").geom("geom1").feature(Line).set("
    specify2", "coord");
model.component("comp1").geom("geom1").feature(Line).set("
    coord1", new double[]{OD[0][0]/2, create_foils[0][1]}); //
     Start point, r motsvarar x-axeln och z is y-axeln
model.component("comp1").geom("geom1").feature(Line).set("
    coord2", new double[]{OD[0][0]/2, create_foils[0][4]}); //
     End point
model.component("comp1").geom("geom1").run(Line); // Creating
     line

// Line between the upper foil and the conductor
String LineU = "LU";
model.component("comp1").geom("geom1").create(LineU, "
    LineSegment"); //Creating geometry object
model.component("comp1").geom("geom1").feature(LineU).set("
    specify1", "coord"); //Setting geometry object features
model.component("comp1").geom("geom1").feature(LineU).set("
    specify2", "coord");
model.component("comp1").geom("geom1").feature(LineU).set("
    coord1", new double[]{OD[0][0]/2, create_foils[0][1]}); //
     Start point, r motsvarar x-axeln och z is y-axeln
model.component("comp1").geom("geom1").feature(LineU).set("
    coord2", new double[]{create_foils[0][0]/2, create_foils
    [0][1]}); // End point
model.component("comp1").geom("geom1").run(LineU); //
    Creating line

// Line between the lower foil and the conductor
String LineL = "LL";
model.component("comp1").geom("geom1").create(LineL, "
    LineSegment"); //Creating geometry object
model.component("comp1").geom("geom1").feature(LineL).set("
    specify1", "coord"); //Setting geometry object features
model.component("comp1").geom("geom1").feature(LineL).set("
    specify2", "coord");
model.component("comp1").geom("geom1").feature(LineL).set("
    coord1", new double[]{OD[0][0]/2, create_foils[0][4]}); //
     Start point, r motsvarar x-axeln och z is y-axeln
model.component("comp1").geom("geom1").feature(LineL).set("
    coord2", new double[]{create_foils[0][0]/2, create_foils
    [0][4]}); // End point
model.component("comp1").geom("geom1").run(LineL); //
    Creating line
```

```
//-------------------------------------------------------------
// 4. Create line between partial create_foils on the inner
   side

// Drawing lines over full create_foils on the upper side
for (int k = 0; k < rows-2; k++) {
  if (create_foils[k][2] == create_foils[k][3] && k > 2 &&
     create_foils[k+1][2] != create_foils[k+1][3]) { // Check
      if it is a full foil
    String UpperLine5 = k+"doubleU"; // A line between two
       partial create_foils if there is a full foil in
       between
    model.component("comp1").geom("geom1").create(UpperLine5,
        "LineSegment"); //Creating geometry object
    model.component("comp1").geom("geom1").feature(UpperLine5
       ).set("specify1", "coord"); //Setting geometry object
       features
    model.component("comp1").geom("geom1").feature(UpperLine5
       ).set("specify2", "coord");
    model.component("comp1").geom("geom1").feature(UpperLine5
       ).set("coord1", new double[]{create_foils[k-1][0]/2,
       create_foils[k-1][2]}); // Start point
    model.component("comp1").geom("geom1").feature(UpperLine5
       ).set("coord2", new double[]{create_foils[k+1][0]/2,
       create_foils[k+1][2]}); // End point
    model.component("comp1").geom("geom1").run(UpperLine5);
  }
}
// Drawing lines between partial create_foils on the upper
   side
for (int k = 0; k < rows-1; k++) {
  if (create_foils[k][2] != create_foils[k][3] &&
     create_foils[k+1][2] != create_foils[k+1][3]) { // Check
      if it is a partial foil and that the next one is a
      partial foil
    String UpperLine0 = k+"simpleU"; // A line between two
       partial create_foils
    model.component("comp1").geom("geom1").create(UpperLine0,
        "LineSegment"); //Creating geometry object
    model.component("comp1").geom("geom1").feature(UpperLine0
       ).set("specify1", "coord"); //Setting geometry object
       features
    model.component("comp1").geom("geom1").feature(UpperLine0
       ).set("specify2", "coord");
    model.component("comp1").geom("geom1").feature(UpperLine0
       ).set("coord1", new double[]{create_foils[k][0]/2,
       create_foils[k][2]}); // Start point
    model.component("comp1").geom("geom1").feature(UpperLine0
       ).set("coord2", new double[]{create_foils[k+1][0]/2,
```

```
        create_foils[k+1][2]}); // End point
    model.component("comp1").geom("geom1").run(UpperLine0);
  }
}

//------------------------------------------------------------
// Drawing lines over full create_foils on the lower side
for (int k = 0; k < rows-2; k++) {
  if (create_foils[k][2] == create_foils[k][3] && k > 2 &&
     create_foils[k+1][2] != create_foils[k+1][3]) { // Check
      if it is a full foil
    String UpperLine5 = k+"doubleL"; // A line between two
       partial create_foils if there is a full foil in
       between
    model.component("comp1").geom("geom1").create(UpperLine5,
        "LineSegment"); //Creating geometry object
    model.component("comp1").geom("geom1").feature(UpperLine5
       ).set("specify1", "coord"); //Setting geometry object
       features
    model.component("comp1").geom("geom1").feature(UpperLine5
       ).set("specify2", "coord");
    model.component("comp1").geom("geom1").feature(UpperLine5
       ).set("coord1", new double[]{create_foils[k-1][0]/2,
       create_foils[k-1][3]}); // Start point
    model.component("comp1").geom("geom1").feature(UpperLine5
       ).set("coord2", new double[]{create_foils[k+1][0]/2,
       create_foils[k+1][3]}); // End point
    model.component("comp1").geom("geom1").run(UpperLine5);
  }
}
// Drawing lines between partial create_foils on the lower
   side
for (int k = 0; k < rows-1; k++) {
  if (create_foils[k][2] != create_foils[k][3] &&
     create_foils[k+1][2] != create_foils[k+1][3]) { // Check
      if it is a partial foil and that the next one is a
     partial foil
    String UpperLine0 = k+"simpleL"; // A line between two
       partial create_foils
    model.component("comp1").geom("geom1").create(UpperLine0,
        "LineSegment"); //Creating geometry object
    model.component("comp1").geom("geom1").feature(UpperLine0
       ).set("specify1", "coord"); //Setting geometry object
       features
    model.component("comp1").geom("geom1").feature(UpperLine0
       ).set("specify2", "coord");
    model.component("comp1").geom("geom1").feature(UpperLine0
       ).set("coord1", new double[]{create_foils[k][0]/2,
       create_foils[k][3]}); // Start point
```

```
    model.component("comp1").geom("geom1").feature(UpperLine0
        ).set("coord2", new double[]{create_foils[k+1][0]/2,
        create_foils[k+1][3]}); // End point
    model.component("comp1").geom("geom1").run(UpperLine0);
  }
}
```

A.2 Deletion of Foils in Bushing Geometry

```
//Method that deletes the foils.
// Get data from Excel
String[][] delete_foils = readExcelFile("
    GSB800_ext06_olin_FOD_FOD6210_10% _20230109_enligt
    lindningsritning.xlsm", "ANALYSIS", "D16"); // Needs to be
     same input as "CreateFoils" method.

// Remove the single lines to the conductor
model.component("comp1").geom("geom1").feature().remove("L");
     //Remove the line on the outer rectangle
model.component("comp1").geom("geom1").feature().remove("LU")
    ; //Remove the upper line between the outer rectangle and
    the foil
model.component("comp1").geom("geom1").feature().remove("LL")
    ; //Remove the lower line between the outer rectangle and
    the foil


// Removing every foil
int rows = delete_foils.length;
for (int i = 0; i < rows; i++) { // looping over every row (#
    rows = #foils)
  try { // Remove full foil object
    model.component("comp1").geom("geom1").feature().remove("
        bF"+i+" full"); //Removing the full foil
    model.component("comp1").geom("geom1").selection().remove
        ("selFF"+i); //Full foil
  }
  catch (Exception e1) { // If no full foil object ==> two
      partial foils are removed instead.
    model.component("comp1").geom("geom1").feature().remove("
        b"+i+" partial upp"); //Removing partial foil
    model.component("comp1").geom("geom1").selection().remove
        ("selPFU"+i); // removing cumulative selection of the
        upper partial foil
    model.component("comp1").geom("geom1").feature().remove("
        b"+i+" partial low"); //Removing partial foil
```

```
    model.component("comp1").geom("geom1").selection().remove
       ("selPFL"+i); // removing cumulative selection of the
       lower partial foil
  }
}



//------------------------------------------------------------
// Removing every upper line between foils
for (int j = 0; j < rows-1; j++) {
  model.component("comp1").geom("geom1").feature().remove("L"
     +j+" upper line");
  model.component("comp1").geom("geom1").feature().remove("L"
     +j+" lower line");
}

// Removing lines on the inside of the parial foils
int columns = 5;
double[][] excelData = new double[rows][columns]; // message(
   excelData);

// Turning string matrix into matrix with numbers using for
   loops. For tube/foil
for (int i = 0; i < rows; i++) { //looping over every row
  for (int j = 0; j < columns; j++) {
    double value = Double.parseDouble(delete_foils[i][j]); //
       Changing type from String to Double.
    double scale = 0.001; //Excel sheet value is in [mm].
       Scaling to [m] for COMSOL
    excelData[i][j] = value*scale; //Changing [mm] to [m]
  }
}

//------------------------------------------------------------
// Removing every line between foils on the inside of the
   partial foils
for (int k = 0; k < rows-2; k++) {
  if (excelData[k][2] == excelData[k][3] && k > 2 &&
     excelData[k+1][2] != excelData[k+1][3]) { // Checking if
      there is a full foil between the partial foils
    model.component("comp1").geom("geom1").feature().remove(k
       +"doubleU"); // Remove the line overlapping a full
       foil on the upper side
    model.component("comp1").geom("geom1").feature().remove(k
       +"doubleL"); // Remove the line overlapping a full
       foil on the lower side
  }
}
```

```
for (int k = 0; k < rows-1; k++) {
  if (excelData[k][2] != excelData[k][3] && excelData[k+1][2]
      != excelData[k+1][3]) { // Checking if it is a partial
     foil and the next one in a partial foil
    model.component("comp1").geom("geom1").feature().remove(k
       +"simpleU"); // Remove line between partial foils on
       the upper side
    model.component("comp1").geom("geom1").feature().remove(k
       +"simpleL"); // Remove line between partial foils on
       the lower side
  }
}

model.component("comp1").geom("geom1").nodeGroup().remove("
   grp1");
model.component("comp1").geom("geom1").nodeGroup().remove("
   grp2");
model.component("comp1").geom("geom1").nodeGroup().remove("
   grp3");
```

A.3 Assigning Floating Potential to Foils

```
// Code for assigning potentials to the foils

// Read data from Excel
String[][] foil_parameters = readExcelFile("
   GSB800_ext06_olin_FOD_FOD6210_10% _20230109_enligt
   lindningsritning.xlsm", "ANALYSIS", "D16"); // diameter
   and length of foils

int rows = foil_parameters.length; //Number of rows in excel
   sheet "ANALYSIS", equals number of foils
int columns = 5;
double[][] flo_pot_foils = new double[rows][columns];

// Turning string matrix into matrix with numbers using for
   loops. For tube/foil
for (int i = 0; i < rows; i++) { //looping over every row
  for (int j = 0; j < columns; j++) {
    double value = Double.parseDouble(foil_parameters[i][j]);
       //Changing type from String to Double.
    double scale = 0.001; //Excel sheet value is in [mm].
       Scaling to [m] for COMSOL
    flo_pot_foils[i][j] = value*scale; //Changing [mm] to [m]
  }
```

```
}

//Creating the physics "ELECTROSTATICS"
model.component("comp1").physics().create("es", "
   Electrostatics", "geom1");
model.nodeGroup().create("grp3", "Physics", "es");
model.nodeGroup("grp3").label("Floating_Potential_Full_Foil")
   ;
model.nodeGroup().create("grp4", "Physics", "es");
model.nodeGroup("grp4").label("
   Floating_Potential_Partial_Upper_Foil");

model.nodeGroup().create("grp5", "Physics", "es");
model.nodeGroup("grp5").label("
   Floating_Potential_Partial_Lower_Foil");
//

// Adding a potential to each foil depending on if it is a
   full, upper partial or lower partial foil

for (int k = 1; k < rows; k++) {
if (flo_pot_foils[k][2] == flo_pot_foils[k][3]) { // Add
   potential to a full foil
     // String potFull = "potFF"+k; // Object for the
        electric potential
    // String nameFF = "geom1_selFF"+k+"_bnd"; // Name for
       the electric potential
    String potF = "potF"+k; // Object for the floating
       potential
    String nameF = "geom1_selFF"+k+"_bnd"; // Name for the
       floating potential
    // model.component("comp1").physics("es").create(potFull,
        "ElectricPotential", 1); // Adding electric potential
   //model.component("comp1").physics("es").feature(potFull).
      selection().named(nameFF);
model.component("comp1").physics("es").create(potFull, "
   ElectricPotential", 1); // Adding electric potential
model.component("comp1").physics("es").feature(potFull).
   selection().named(nameFF);
model.component("comp1").physics("es").create(potF, "
   FloatingPotential", 1); // Adding floating potential
model.nodeGroup("grp3").add(potF);
model.component("comp1").physics("es").feature(potF).
   selection().named(nameF);   model.component("comp1").
   physics("es").feature(potF).label("
   Floating_Potential_Full_Foil_"+k);
/} else {
// Add potential to the upper partial foils
String potU = "potUPF"+k; // UPF = Upper Partial Foil
```

```
String nameU = "geom1_selPFU"+k+"_bnd"; // Name of the
    potential for the upper partial foil
model.component("comp1").physics("es").create(potU, "
    FloatingPotential", 1);
 model.nodeGroup("grp4").add(potU);  model.component("comp1")
     .physics("es").feature(potU).selection().named(nameU);
     model.component("comp1").physics("es").feature(potU).
     label("Floating_Potential_Partial_Upper_Foil_"+k);

// Add potential to the lower partial foils
String potL = "potLPF"+k; // LPF = Lower Partial Foil
     String nameL = "geom1_selPFL"+k+"_bnd";
     model.component("comp1").physics("es").create(potL, "
        FloatingPotential", 1);
     model.nodeGroup("grp5").add(potL);     model.component("
        comp1").physics("es").feature(potL).selection().named(
        nameL); model.component("comp1").physics("es").feature
        (potL).label("Floating_Potential_Partial_Lower_Foil_"+
        k);
  }
}

// Creating the physics "ELECTRIC CURRENTS"

model.nodeGroup().create("grp6", "Physics", "ec");
model.nodeGroup("grp6").label("Floating_Potential_Full_Foil_1
    ");

model.nodeGroup().create("grp7", "Physics", "ec");
model.nodeGroup("grp7").label("
    Floating_Potential_Partial_Upper_Foil_1");

model.nodeGroup().create("grp8", "Physics", "ec");
model.nodeGroup("grp8").label("
    Floating_Potential_Partial_Lower_Foil_1");


// Adding a potential to each foil depending on if it is a
    full, upper partial or lower partial foil

for (int k = 1; k < rows; k++) {
  if (flo_pot_foils[k][2] == flo_pot_foils[k][3]) { // Add
      potential to a full foil
     // String potFull = "potFF"+k; // Object for the electric
         potential
     // String nameFF = "geom1_selFF"+k+"_bnd"; // Name for
        the electric potential
     String potF = "potF"+k; // Object for the floating
        potential
```

```
    String nameF = "geom1_selFF"+k+"_bnd"; // Name for the
       floating potential
    // model.component("comp1").physics("ec").create(potFull,
        "ElectricPotential", 1); // Adding electric potential
    // model.component("comp1").physics("ec").feature(potFull
       ).selection().named(nameFF);
    model.component("comp1").physics("ec").create(potF, "
       FloatingPotential", 1); // Adding floating potential
    model.nodeGroup("grp6").add(potF);
    model.component("comp1").physics("ec").feature(potF).
       selection().named(nameF);
    model.component("comp1").physics("ec").feature(potF).
       label("Floating_Potential_Full_Foil_1-"+k);
  } else {
    // Add potential to the upper partial foils
    String potU = "potUPF"+k; // UPF = Upper Partial Foil
    String nameU = "geom1_selPFU"+k+"_bnd"; // Name of the
       potential for the upper partial foil
    model.component("comp1").physics("ec").create(potU, "
       FloatingPotential", 1);
    model.nodeGroup("grp7").add(potU);
    model.component("comp1").physics("ec").feature(potU).
       selection().named(nameU);
    model.component("comp1").physics("ec").feature(potU).
       label("Floating_Potential_Partial_Upper_Foil_1-"+k);


    // Add potential to the lower partial foils
    String potL = "potLPF"+k; // LPF = Lower Partial Foil
    String nameL = "geom1_selPFL"+k+"_bnd";
    model.component("comp1").physics("ec").create(potL, "
       FloatingPotential", 1);
    model.nodeGroup("grp8").add(potL);
    model.component("comp1").physics("ec").feature(potL).
       selection().named(nameL);
    model.component("comp1").physics("ec").feature(potL).
       label("Floating_Potential_Partial_Lower_Foil_1-"+k);
  }
}
```

A.4 Deleting Floating Potential from Foils

```
// Delete the electrostatics-section
model.component("comp1").physics("es").feature().remove("es")
   ;
```

```
//-------------------------------------------------------------
// Get data from Excel
String[][] foil_parameters = readExcelFile("
   GSB800_ext06_olin_FOD_FOD6210_10% _20230109_enligt
   lindningsritning.xlsm", "ANALYSIS", "D16"); // diameter
   and length of foils

int rows = foil_parameters.length; //Number of rows in excel
   sheet "ANALYSIS", equals number of foils
int columns = 5;
double[][] del_flo_pot_foils = new double[rows][columns];

// Turning string matrix into matrix with numbers using for
   loops. For tube/foil

for (int i = 0; i < rows; i++) { //looping over every row
  for (int j = 0; j < columns; j++) {
    double value = Double.parseDouble(foil_parameters[i][j]);
        //Changing type from String to Double.
    double scale = 0.001; //Excel sheet value is in [mm].
       Scaling to [m] for COMSOL
    del_flo_pot_foils[i][j] = value*scale; //Changing [mm] to
        [m]
  }
}

// Deleting the potential of each foil depending on if it is
   a full, upper partial or lower partial foil

for (int k = 1; k < rows; k++)
{
  if (del_flo_pot_foils[k][2] == del_flo_pot_foils[k][3]) {
     // delete potential to a full foil

    model.component("comp1").physics("es").feature().remove("
       potF"+k);
    model.component("comp1").physics("ec").feature().remove("
       potF"+k);
  }

  else
  {
    model.component("comp1").physics("es").feature().remove("
       potUPF"+k); // removing potential to the upper partial
        foils

    model.component("comp1").physics("es").feature().remove("
       potLPF"+k); // removing potential to the lower partial
```

```
        foils

    model.component("comp1").physics("ec").feature().remove("
       potUPF"+k); // removing potential to the upper partial
        foils

    model.component("comp1").physics("ec").feature().remove("
       potLPF"+k); // removing potential to the lower partial
        foils

  }
}

model.nodeGroup().remove("grp3");
model.nodeGroup().remove("grp4");
model.nodeGroup().remove("grp5");

model.nodeGroup().remove("grp6");
model.nodeGroup().remove("grp7");
model.nodeGroup().remove("grp8");
```

DEPARTMENT OF SOME SUBJECT OR TECHNOLOGY
CHALMERS UNIVERSITY OF TECHNOLOGY
Gothenburg, Sweden
www.chalmers.se

CHALMERS
UNIVERSITY OF TECHNOLOGY